SUBSONIC AND SUPERSONIC FLUTTER ANALYSIS OF A HIGHLY TAPERED SWEPT-WING PLANFORM, INCLUDING EFFECTS OF DENSITY VARIATION AND FINITE WING THICKNESS, AND COMPARISON WITH EXPERIMENTS

by E. Carson Yates, Jr.

Langley Research Center

Langley Station, Hampton, Va.

SUBSONIC AND SUPERSONIC FLUTTER ANALYSIS OF A

HIGHLY TAPERED SWEPT-WING PLANFORM, INCLUDING

EFFECTS OF DENSITY VARIATION AND FINITE WING

THICKNESS, AND COMPARISON WITH EXPERIMENTS

By E. Carson Yates, Jr.

Langley Research Center
Langley Station, Hampton, Va.

NATIONAL AERONAUTICS AND SPACE ADMINISTRATION

SUBSONIC AND SUPERSONIC FLUTTER ANALYSIS OF A

HIGHLY TAPERED SWEPT-WING PLANFORM, INCLUDING

EFFECTS OF DENSITY VARIATION AND FINITE WING

THICKNESS, AND COMPARISON WITH EXPERIMENTS*

By E. Carson Yates, Jr.

Langley Research Center

SUMMARY

The flutter characteristics of several wings with an aspect ratio of 4.0, a taper ratio of 0.2, and a quarter-chord sweepback of 45° have been investigated analytically for Mach numbers up to 2.0. The calculations were based on the modified-strip-analysis method, the subsonic-kernel-function method, piston theory, and quasi-steady second-order theory. Results of the analysis and comparisons with experiment indicated that: (1) Flutter speeds were accurately predicted by the modified strip analysis, although accuracy at the highest Mach numbers required the use of nonlinear aerodynamic theory (which accounts for effects of wing thickness) for the calculation of the aerodynamic parameters. (2) An abrupt increase of flutter-speed coefficient with increasing Mach number, observed experimentally in the transonic range, was also indicated by the modified strip analysis. (3) In the low supersonic range for some densities, a discontinuous variation of flutter frequency with Mach number was indicated by the modified strip analysis. An abrupt change of frequency appeared experimentally in the transonic range. (4) Differences in flutter-speed-coefficient levels obtained from tests at low supersonic Mach numbers in two wind tunnels were also predicted by the modified strip analysis and were shown to be caused primarily by differences in mass ratio. (5) Flutter speeds calculated by the subsonic-kernel-function method were in good agreement with experiment and with the results of the modified strip analysis. (6) Flutter speeds obtained from piston theory and from quasi-steady second-order theory were higher than experimental values by at least 38 percent.

INTRODUCTION

Subsonic, transonic, and supersonic flutter tests of several highly tapered swept wings have been conducted in the Langley transonic blowdown tunnel (e.g., see refs. 1 to 3) and in the Langley 9- by 18-inch supersonic aeroelasticity

---

tunnel (ref. 3 and unpublished data) for Mach numbers up to 2.55. These data have indicated (1) an abrupt and rather large increase of both flutter-speed coefficient and flutter-frequency ratio with increasing Mach number in the transonic range and (2) an apparent discrepancy at low supersonic Mach numbers between flutter-speed coefficient levels obtained in the two tunnels.

In order to study these flutter characteristics in more detail, comprehensive modal-type flutter analyses have been made for the wings employed in the transonic blowdown tunnel tests reported in reference 1 and in an unpublished investigation conducted in the Langley 9- by 18-inch supersonic aeroelasticity tunnel for Mach numbers up to 2.0. These thin, homogeneous wings had an aspect ratio of 4.0, a taper ratio of 0.2, a quarter-chord sweepback of 45°, and NACA 65A-series airfoil sections. The geometric, mass, and stiffness properties of these wings are given in appendix A. The primary objectives of this study were (1) to determine whether the sudden change of flutter behavior at transonic speeds could be predicted, (2) to formulate, if possible, an explanation for the differences between the flutter data obtained in the two tunnels, and (3) to examine the relative accuracies of several methods of flutter calculation.

The majority of the flutter calculations presented herein were made by the modified-strip-analysis method of reference 4. A refinement in the evaluation of the aerodynamic parameters employed in this method is introduced in appendix B in order to represent more accurately the load distribution on highly tapered wings. In addition, the effects of finite wing thickness in flutter calculations for the higher supersonic Mach numbers are illustrated. Since the two previously mentioned test facilities operate at appreciably different density levels, the importance of this density variation has been examined in the present analysis. An illustration of some effects of tunnel operating conditions on measured flutter boundaries is included in appendix C.

Some calculations by the modified-strip-analysis method are also presented for two of the configurations of reference 2. These wings are the same as those of reference 1, except that ballast weights were added along the leading edge in an attempt to raise the flutter speed.

Finally, for comparison purposes, some flutter calculations have been made for the wings of reference 1 by the subsonic-kernel-function method (ref. 5) and for the wing tested in the Langley 9- by 18-inch supersonic aeroelasticity tunnel by piston theory (e.g., refs. 6 to 8) and by quasi-steady second-order theory (e.g., refs. 8 and 9) for Mach numbers from 1.7 to 2.0.

SYMBOLS

$a_{c,n}$ nondimensional distance from midchord to local aerodynamic center (for steady flow) measured perpendicular to elastic axis, positive rearward; fraction of local semichord perpendicular to elastic axis

b_r semichord of wing measured perpendicular to elastic axis at spanwise reference station $\eta = 0.75$

2

b_s semichord measured streamwise at wing panel root

$c_{l_{\alpha,n}}$ local lift-curve slope for a section perpendicular to elastic axis in steady flow

$c_{m_{\alpha,n}}$ derivative with respect to angle of attack of local pitching-moment coefficient measured about leading edge of a section perpendicular to elastic axis in steady flow

g coefficient of structural damping required to maintain harmonic oscillation at a particular reduced frequency

h_i modal deflection of wing in ith uncoupled bending mode (normalized translational displacement of wing measured at elastic axis)

M Mach number

$\bar{m}$ total mass of exposed wing panel

Δp lifting pressure

T static temperature

V flutter speed

V_R calculated reference flutter speed obtained from modified-strip-analysis method by using aerodynamic parameters for two-dimensional incompressible flow

v volume of air within a conical frustum having streamwise root chord as lower base diameter, streamwise tip chord as upper base diameter, and panel span as height

$\bar{x}$ streamwise distance from wing leading edge, positive rearward; fraction of local chord

$\bar{y}$ spanwise distance from wing panel root, fraction of panel span

z_j normalized local translational displacement of wing in jth coupled mode

α modal deflection of wing in first uncoupled torsion mode (normalized angular displacement of wing measured about elastic axis)

η distance measured from wing panel root along elastic axis, fraction of elastic-axis length

Λ_{ea} sweep angle of wing elastic axis

$\bar{\mu}$ mass ratio for exposed wing panel, $\bar{m}/\rho v$

ρ air density

ω circular frequency of vibration at flutter

ω_k circular frequency of kth coupled vibration mode

$\omega_{h,i}$ circular frequency of ith uncoupled bending vibration mode

ω_α circular frequency of first uncoupled torsional vibration mode

Subscripts:

2D   two dimensional

3D   three dimensional

DESCRIPTION OF WINGS

All wing panels analyzed in this investigation represented wings with a full-span aspect ratio of 4.0, a full-wing taper ratio ·of 0.2, a quarter-chord sweepback of 45°, and NACA 65A-series airfoil sections streamwise. All were of essentially homogeneous construction except those with added ballast along the leading edge. (See ref. 2.) The wings differed slightly in panel aspect ratio and panel taper ratio because of the presence or absence of a simulated fuselage. Differences also occurred in thickness ratio and in the presence, location, and amount of leading-edge ballast. Further details of wing geometry are given in table I, figure 1, and appendix A. Model properties are also discussed in appendix A, and the modal frequencies are summarized in table II. For convenience, the wing designations used in references 1 and 2 are retained herein, and the half-span wing tested in the Langley 9- by 18-inch supersonic aeroelasticity tunnel (results unpublished) is designated model B.

FLUTTER ANALYSIS

In this investigation, all calculated flutter points were determined from conventional graphs of required structural damping plotted against airspeed (V-g plots). For an n-mode calculation, n curves are traced out in the V-g plot by the solutions of the n-by-n flutter determinant with reduced frequency as the independently varying parameter. Since the pertinent structural damping values are not known for the models used in this investigation, and since the damping coefficients for homogeneous wings of the present type are usually very small, all calculated flutter points are taken to be points for which $g = 0$.

An index to the types of calculations made, the vibration modes employed, and the results of the analyses is given in table III.

4

Modified Strip Analysis

Preliminary flutter calculations made by the modified strip method (appendix B) have indicated that for the analyses of the present highly tapered wings: (1) The required steady-flow aerodynamic parameters should be evaluated by direct integration of lifting pressures along wing sections perpendicular to the elastic axis. (2) Use in the analyses of three vibration modes should be sufficient. (3) Separate representative flow densities should be used in the subsonic and supersonic Mach number ranges. These three requirements have been followed in all of the final flutter calculations made by the modified strip method.

The final flutter calculations employed values of steady-flow aerodynamic parameters computed from subsonic (ref. 10) or supersonic (refs. 11 and 12) linearized lifting-surface theory. In addition to the flutter calculations based on linearized aerodynamic theory, one calculation for model B at $M = 2.0$ employed an aerodynamic correction for finite wing thickness based on the Busemann second-order theory. No general theory is known to exist for evaluating the nonlinear aerodynamic effects of finite wing thickness on the supersonic steady-flow aerodynamic loads on finite-span wings. For use in the present flutter analysis, therefore, such nonlinear effects were approximated by employing the two-dimensional Busemann second-order theory to modify the spanwise distributions of aerodynamic parameters calculated from three-dimensional linearized theory. Specifically, the values of section pitching-moment slope $c_{m_{\alpha},n}$ obtained from three-dimensional linear theory were multiplied by the ratio of $c_{m_{\alpha},n}$ obtained from the two-dimensional nonlinear theory to $c_{m_{\alpha},n}$ obtained from two-dimensional linear theory; that is,

$$\left(c_{m_{\alpha},n}\right)_{3D,\text{ second order}} = \left[\frac{\left(c_{m_{\alpha},n}\right)_{2D,\text{ second order}}}{\left(c_{m_{\alpha},n}\right)_{2D,\text{ linear}}}\right]\left(c_{m_{\alpha},n}\right)_{3D,\text{ linear}}$$

A similar procedure for the section lift-curve slope, however, leaves values of $c_{l_{\alpha},n}$ unchanged. That is,

$$\left(c_{l_{\alpha},n}\right)_{3D,\text{ second order}} = \left[\frac{\left(c_{l_{\alpha},n}\right)_{2D,\text{ second order}}}{\left(c_{l_{\alpha},n}\right)_{2D,\text{ linear}}}\right]\left(c_{l_{\alpha},n}\right)_{3D,\text{ linear}}$$

$$\equiv \left(c_{l_{\alpha},n}\right)_{3D,\text{ linear}}$$

Local aerodynamic-center positions are given by

$$\left(a_{c,n}\right)_{3D,\text{ second order}} = 2\left[\frac{\left(c_{m_{\alpha},n}\right)_{3D,\text{ second order}}}{\left(c_{l_{\alpha},n}\right)_{3D,\text{ second order}}}\right] - 1$$

The resulting correction to linear theory, which is a function only of Mach number and of the airfoil cross-sectional area, yields a forward shift of local aerodynamic center. The Busemann second-order theory, rather than the complete shock-expansion theory, was employed here because of the complications which are encountered in applying the shock-expansion theory to airfoils with round leading edges. Analogous calculations employing both theories for some thin wings with sharp leading edges have shown that for a given Mach number, the aerodynamic centers calculated by shock-expansion theory are slightly farther forward than those given by Busemann second-order theory.

Distributions of the aerodynamic parameters $c_{l_{\alpha,n}}$ and $a_{c,n}$ used in flutter calculations for model 1-left are shown in figure 2 for ten Mach numbers and for model B in figure 3 for six Mach numbers. Corresponding quantities for models 4A-right, ballast I, and ballast II are similar to those shown for model 1-left. Some small numerical differences occur, however, because of different elastic-axis positions. All the final modified-strip-theory calculations employed three calculated uncoupled vibration modes (first torsion and first and second bending) as indicated in table III.

Subsonic Kernel Function

The subsonic-kernel-function calculations for models 4A-right and 2A-left followed the procedure described in reference 5. Nine downwash collocation points were used in each calculation. These points were taken at 30, 60, and 90 percent of the panel span and at 25, 50, and 75 percent of the local streamwise chord. Kernel-function analyses for other wings have indicated that the calculated flutter characteristics generally are not very sensitive to small changes in the positions of these collocation points.

All kernel-function calculations for model 4A-right employed calculated uncoupled first torsion mode and first and second bending modes. The associated modal frequencies are shown in table II. All calculations for model 2A-left used the first three calculated coupled mode shapes and frequencies as shown in figure 4 and table II. Neither coupled nor uncoupled modes were assumed to be orthogonal, and the cross-product generalized masses were retained in the flutter determinant.

Piston Theory and Quasi-Steady Second-Order Theory

The piston-theory and second-order-theory calculations for model B were similar to the subsonic-kernel-function calculations, except that the generalized aerodynamic forces were formulated from the lifting-pressure expression given in equation (16) of reference 8. As indicated in reference 8, the lifting pressure expressions for piston theory and for quasi-steady second-order theory differ only with respect to two coefficients which depend only on Mach number and the ratio of specific heats. All of the calculations based on these two theories include the effect of finite wing thickness.

Both coupled-mode and uncoupled-mode analyses were made for model B. (See table III.) As indicated in appendix A, the three uncoupled modes (first torsion and first and second bending) were calculated by the method of reference 13, whereas the first three coupled modes were measured. (See fig. 5.) For both types of modes, however, the modal frequencies were obtained from measured values. (See table II.)

Piston theory and quasi-steady second-order theory as expressed in reference 8 and as applied herein take no account of streamwise wing tips except as a limit to the region of integration. However, for some of the calculations shown herein, an approximate tip correction was made on the basis of steady-flow linear theory. (See ref. 12.) The streamwise tip, of course, influences loading only within the triangular region bounded by the tip, the trailing edge, and the Mach line from the leading-edge tip. It may be noted that because the present wings are swept and highly tapered, this tip triangle covers only a small portion of the wing panel, and its area decreases as Mach number increases. Furthermore, the reduced frequency at flutter characteristically decreases as Mach number increases so that a steady-flow type of tip correction should be more accurate at the higher Mach numbers. The tip correction as applied herein consists of multiplying the piston-theory or second-order theory loading at each point within the tip triangle by the ratio of steady-state load with streamwise tip to steady-state load without streamwise tip, both being for the undeformed wing. For a given wing, this ratio, of course, varies with the location of the point within the tip triangle and with Mach number. Thus for piston theory, for example, the corrected lifting pressure at a point $\bar{x},\bar{y}$ on the wing is given by

$$\Delta p(\bar{x},\bar{y},M)_{\text{piston theory corrected}}$$

$$= \Delta p(\bar{x},\bar{y},M)_{\text{piston theory uncorrected}} \left[\frac{\Delta p(\bar{x},\bar{y},M)_{\text{linear theory with tip}}}{\Delta p(\bar{x},\bar{y},M)_{\text{linear theory without tip}}} \right]$$

PRESENTATION OF RESULTS

In order to determine whether the experimentally observed sudden change in flutter behavior at transonic speeds is also theoretically indicated, flutter calculations have been made for models 1-left and 4A-right by the modified strip method of reference 1. The resulting flutter-speed coefficients and flutter-frequency ratios are compared in figures 6 and 7 with experimental flutter data from reference 1. Figures 8 and 9 show effects of density variation on the calculated flutter speeds and frequencies for models 1-left and 4A-right. Some flutter calculations have been made by the modified strip method for models ballast I and ballast II to show effects of leading-edge ballast on the flutter behavior of wings of the present planform. These calculated flutter speeds and frequencies are compared in figures 10 to 13 with experimental flutter data from reference 2.

In order to examine theoretically the flutter behavior of wings tested in different wind tunnels, some calculations by the modified strip method have been made for model B. The calculated results for model B are compared in figures 14 and 15 with unpublished experimental data and with the measured and calculated flutter characteristics for model 4A-right.

In order to investigate the accuracies of flutter prediction by methods other than the modified strip analysis, flutter calculations have been made for models 4A-right and 2A-left by the subsonic-kernel-function method and for model B by piston theory and by quasi-steady second-order theory. In figures 16 and 17, the subsonic-kernel-function calculations for model 4A-right (uncoupled modes) and for model 2A-left (coupled modes) are compared with results of the modified strip analysis for model 4A-right and with experimental flutter data from reference 1. Finally, figure 18 presents comparisons of piston-theory and quasi-steady second-order theory flutter calculations and experimental flutter data for model B.

Table III gives a summary of the types of flutter calculations made and an index to the results.

DISCUSSION

Modified Strip Analysis

Models 1-left and 4A-right.- Final flutter calculations for models 1-left and 4A-right in figures 6 and 7 show that at subsonic Mach numbers, both the flutter-speed coefficients (fig. 6) and the flutter-frequency ratios (fig. 7) calculated for the two wings are very close together, as had previously been indicated by the experimental flutter data from reference 1. It may be noted that the flow densities used in the subsonic calculations (ρ = 0.0025 slug/cu ft for model 1-left and ρ = 0.0022 slug/cu ft for model 4A-right) correspond to $\bar{\mu}$ = 35.9 for model 1-left and $\bar{\mu}$ = 33.0 for model 4A-right. This difference in mass ratio is small, and the curves of figure 8 show that subsonic flutter-speed coefficients are not very sensitive to changes in mass ratio. However, a comparison of the two wings on the basis of equal mass ratio would bring the subsonic curves of figures 6 and 7 even closer together. Figures 6 and 7 show very good agreement between calculated and experimental values of subsonic flutter-speed coefficient and flutter-frequency ratio.

At supersonic Mach numbers, the curves of flutter-speed coefficient calculated for models 1-left and 4A-right are more separated than at subsonic speeds, although the flutter-frequency ratios remain essentially coincident. For these calculations, $\bar{\mu}$ = 15.0 for model 1-left and $\bar{\mu}$ = 20.8 for model 4A-right. An examination of figure 8 for these $\bar{\mu}$ values indicates that comparison of the two wings on the basis of equal mass ratio would again yield nearly coincident curves of flutter-speed coefficient. It should be noted, however, that the experimental no-flutter points for the 4-percent-thick wings (ref. 1) cover density values up to ρ = 0.0080 slug/cu ft. Therefore, if supersonic flutter points for the 4-percent-thick wings had been obtained, the associated densities

8

would have been greater than this value. According to figure 8(a), the resulting flutter-speed coefficients for such high densities should be even larger than the values shown in figure 6 for model 1-left. Supersonic flutter data for the 3- and 4-percent-thick wings thus would not be expected to be essentially coincident as they were at subsonic Mach numbers. It should be emphasized that these statements are based on consideration of mass-ratio effects only. Since linearized aerodynamic theory was used in the calculations, no aerodynamic effect of thickness variation is included.

The calculations for model 4A-right at $M = \sqrt{2}$ indicated two flutter solutions. The flutter-speed coefficients associated with these two solutions are very close together, and both are in good agreement with experiment. (See fig. 6.) However, the flutter frequency for one solution is close to the frequency level for subsonic flutter, whereas the frequency for the other solution is appreciably higher and is close to the supersonic experimental values. (See fig. 7.) Thus, in this range of speed and density, the wing might flutter at either of two frequencies and hence in either of two modes. The occurrence of the high-frequency flutter for models 1-left and 4A-right was found to depend on both density and Mach number (see figs. 8 and 9), although no attempt has been made to evaluate precisely its maximum density limit for a given Mach number. Under some conditions of density and Mach number, the flutter speeds associated with the two solutions became identical (fig. 8), and a discontinuous change of flutter frequency is thus indicated. In figure 7 an abrupt increase of flutter frequency in the transonic range is also indicated by the experimental data of reference 1.

As shown in figures 19 and 20, the appearance of the high-frequency flutter solution results from an archlike crossing of the $g = 0$ axis, whereas the lower frequency solution results from a monotonic crossing. These figures also show that even for combinations of Mach number and density which do not yield a high-frequency flutter point, one of the curves may arch very close to the $g = 0$ axis. Therefore, small changes in wing properties or aerodynamic parameters, which cause only slight changes in the location of curves in the V-g plot, could have a pronounced effect on the occurrence of the high-frequency flutter solution. Furthermore, in cases such as those shown in figures 19(b) and 20(a), even though the high-frequency flutter is not predicted mathematically, a region of lightly damped motion would be likely. The arching behavior of one curve in the V-g plot was observed for all densities at each supersonic Mach number calculated. The arching curve in each case was the one which at low speeds (high reduced frequencies) was associated with the second bending mode, whereas the monotonic crossing (lower frequency flutter) was associated with the first torsion mode.

Models ballast I and ballast II.- Figures 10 to 13 show that at subsonic Mach numbers, calculated values of flutter-speed coefficient and flutter-frequency ratio for the two wings with leading-edge ballast are in good agreement with the experimental data. At subsonic Mach numbers the experimental points in these figures, however, appear to indicate that both $\dfrac{V}{b_s \omega_\alpha \sqrt{\mu}}$ and $\dfrac{\omega}{\omega_\alpha}$ increase as M decreases, whereas the calculated curves show little change with Mach number. These slope differences appear because the theoretical curves were

calculated for constant density while the experimental flutter data were obtained at varying density. Although the value $\rho = 0.0021$ slug/cu ft used in the calculations for models ballast I and ballast II in the subsonic range is representative of most of the subsonic-experimental-flutter points, the experimental density increases rapidly as Mach number decreases. Thus, the densities for the experimental flutter points at the lowest Mach numbers shown are $\rho = 0.00390$ slug/cu ft for model ballast I and $\rho = 0.00437$ slug/cu ft for model ballast II. Since figures 8 and 9 show that both $\dfrac{V}{b_s\omega_\alpha\sqrt{\bar{\mu}}}$ and $\dfrac{\omega}{\omega_\alpha}$ characteristically increase with increasing ρ (see also ref. 14), the use of increasing density with decreasing subsonic Mach number would be expected to cause the calculated curves of figures 10 to 13 to rise with decreasing Mach number. Closer representation of measured densities in the flutter calculations is shown by the diamond symbols in figures 10 to 13 to account for the apparent slope differences mentioned previously. By comparison, trends of subsonic flutter-speed coefficient with density for models 1-left and 4A-right were much less pronounced than those for models ballast I and ballast II, so that the influences of density variation on the subsonic flutter comparisons (figs. 6 and 7) were much less evident than those of figures 10 to 13.

At supersonic Mach numbers for model ballast I, there are no experimental flutter points for comparison with the calculated flutter characteristics. (See figs. 10 and 11.) However, the calculated flutter speed is somewhat lower than the highest recorded no-flutter points. For the density used in these calculations ($\rho = 0.0060$ slug/cu ft), only one supersonic flutter boundary existed at the Mach numbers covered. For model ballast II, however, two boundaries were found (figs. 12 and 13), and both were substantially higher than the experimental no-flutter points. The intersection of these two boundaries at about $M = 1.2$ (fig. 12) corresponds to a condition at which the wing could flutter at either of two frequencies, and flutter points on opposite sides of this intersection are indicated to have widely different frequencies.

Model B.- In figures 14 and 15 both calculated and measured flutter characteristics for model B are compared with the results shown in figures 6 and 7 for model 4A-right. As in the case of model 4A-right, the calculated flutter-speed coefficients for model B at the lower supersonic Mach numbers are in good agreement with the one experimental point (fig. 14) but the corresponding calculated flutter frequencies are about 20 percent low. In the calculations for model B, the following experimental values of density were used:

M	ρ, slug/cu ft	$\bar{\mu}$
1.30	0.00133	36.0
1.64	.00101	47.4
2.00	.00089	53.8

For other Mach numbers, density was interpolated linearly between these values. For the densities used in the calculations for model B, no second flutter solution was indicated.

It is evident from figure 14 that the differences between experimental values of flutter-speed coefficient for models B and 4A-right are not caused by discrepancies in the measurements but are actually predicted by the theory. These differences are attributed to four factors. First, the major portions of the differences shown appear to be caused by differences in density. For example, at $M = 1.30$ the values $\bar{\mu} = 36.0$ for model B and $\bar{\mu} = 20.8$ for model 4A-right apply to both theoretical and experimental flutter points. An examination of the lower $M = 1.30$ curve of figure 8(a) (since both model 1-left and model B are 4 percent thick) shows approximately the magnitude of difference in flutter-speed coefficient that can be accounted for by this much difference in $\bar{\mu}$. Figure 8 also shows that the higher the Mach number, the more rapidly the flutter-speed coefficient decreases with decreasing density (increasing altitude). Second, the modal frequencies $\omega_{h,2}$ and ω_α for model B are fairly close together, whereas the corresponding values for models 1-left and 4A-right are not. (See table II.) This closeness of modal frequencies would be expected to contribute somewhat to the lowness of the flutter-speed coefficients for model B. Third, because of the presence of the fuselage on models 1-left and 4A-right, the panel aspect ratio for these wings is somewhat smaller than that for model B. (See table I and fig. 1.) This difference would also be expected to raise slightly the flutter-speed coefficients for models 1-left and 4A-right, relative to model B. Fourth, models B and 4A-right differ in airfoil thickness. (See table I.) However, comparisons between figures 8(a) and 8(b) for $M \approx 1.30$ indicate that thickness alone should have an almost negligible effect on flutter-speed coefficient. It should be remembered, though, that at low supersonic Mach numbers all calculations for models 1-left, 4A-right, and B employ linearized aerodynamic theory. Thus, although the mass and stiffness effects of differing thickness are included, any aerodynamic effects are not.

Figures 14 and 15 show that at the higher supersonic Mach numbers grossly erroneous estimates of flutter speed and frequency can result from use of aerodynamic parameters obtained from linearized theory. In these figures, the calculated curves for model B indicate that caution should be observed if linearized aerodynamic theory is used in the modified strip method when the leading edge is supersonic and the local aerodynamic centers are in the vicinity of the local centers of gravity. The abruptness of the rise in the calculated flutter-speed and flutter-frequency curves beginning near $M = 1.66$ is associated with this close approach of local aerodynamic centers to the elastic axis and local centers of gravity. As Mach number increases slightly above $M = 1.66$, the aerodynamic centers calculated from linearized supersonic-flow theory actually move rearward of the elastic axis and centers of gravity over an outboard portion of the wing. Under such conditions a small change in aerodynamic-center location can have a large effect on the section pitching moment about the elastic axis and can even change its sign. In contrast, similar calculations for two homogeneous untapered wings with 15° and 30° of sweepback and with aspect ratios of 5.34 and 4.16, respectively, have shown only a gradual rise of flutter speed with increasing supersonic Mach number. For those wings, however, the elastic axes and local

centers of gravity were at midchord so that the local aerodynamic centers could never be rearward of these locations. Under these conditions, no change of sign in the section pitching moment occurred.

It is well known that linearized aerodynamic theory characteristically predicts aerodynamic-center positions that are too far rearward and that this condition, in turn, may yield excessively high calculated flutter speeds. (See ref. 15, for example.) One approach to this problem is to use aerodynamic parameters based on nonlinear aerodynamic theories, for example, shock-expansion theory or the Busemann second-order theory. Results of such a calculation employing the Busemann second-order theory for model B at $M = 2.00$ are shown in figures 14 and 15. A comparison of the associated linear-theory and second-order-corrected aerodynamic parameters is shown in figure 3(f). The flutter-speed coefficient calculated from the corrected aerodynamic parameters is in excellent agreement with the experimental value at $M = 2.00$, although the calculated flutter frequency is somewhat low. References 14 and 15 show that as the Mach number increases and the local aerodynamic centers move closer to the local centers of gravity, the calculated flutter speed and frequency become increasingly sensitive to small changes in the aerodynamic-center positions. Under these circumstances, accurate flutter prediction requires aerodynamic-center values more accurate than those yielded by linear aerodynamic theory. The present application of the Busemann-second-order-theory correction to the linear-theory aerodynamic-center positions for $M = 2.00$ (fig. 3(f)) moved the aerodynamic centers from behind to ahead of the centers of gravity and hence caused a large reduction in the calculated flutter speed.

Flutter-boundary surface.- In view of the fact that flutter characteristics for a given wing are functions primarily of the two independent variables, mass ratio and Mach number, it should be helpful and instructive to view the flutter boundary as a surface rather than more conventionally as a line. This surface for a given wing may be traced out by the flutter-speed coefficient $\dfrac{V}{b_s \omega_\alpha \sqrt{\bar{\mu}}}$ (or flutter-frequency ratio $\dfrac{\omega}{\omega_\alpha}$) plotted as a function of the variables Mach number M and mass ratio $\bar{\mu}$. (See fig. 21.) Cross sections of such surfaces for constant values of M are shown in figures 8 and 9 of this report and figures 59 to 80 of reference 14. Sections for constant values of $\bar{\mu}$ are shown, for example, by the calculated curves of figures 6 and 7 of this report and figures 81 to 104 of reference 14. Some effects of variations in mass ratio and the concept of a flutter-speed surface are discussed in reference 16 in connection with two-dimensional flutter problems. The importance of mass ratio in the dynamic scaling of flutter models has long been recognized.

In a three-dimensional presentation of this sort a flutter boundary for a given lifting surface measured in a given facility would generally appear as a single curve or narrow band lying on the flutter-speed surface.[1] (See, e.g., the data of ref. 1.) Tests of the same wing in a different facility may trace

---

[1] If tunnel temperature were independently controllable over a wide range, a broader area of the flutter-speed surface could be covered experimentally.

out a different curve on the flutter-speed surface. Such differences may occur, for example, because of temperature differences between the two tunnels, or because of differences between the properties of the two test media. Thus, projection of data from two facilities onto the $\dfrac{V}{b_s \omega_\alpha \sqrt{\mu}}$, M plane may yield flutter points which do not form a continuous curve. (See, e.g., fig. 14.) Similarly, flutter conditions associated with flight in the atmosphere would also appear on the flutter-speed surface as a single curve which may or may not be closely approximated by tests in a given facility. The implications of the foregoing discussion with regard to the effects on flutter data of wind-tunnel operating conditions and wing size are examined in further detail in appendix C.

Subsonic Kernel Function

Flutter speeds and frequencies calculated by the subsonic-kernel-function method (ref. 5) for models 4A-right and 2A-left are compared in figures 16 and 17 with experimental data and with the modified-strip-analysis calculations previously discussed. Although kernel-function flutter calculations were made only for the two 3-percent-thick wings, measured flutter points for both 3- and 4-percent-thick wings are included in figures 16 and 17 for continuity because both experiments and modified-strip-method calculations (fig. 6) indicate insignificant effects of thickness in the subsonic range.

Model 4A-right.- Calculations for model 4A-right employed calculated uncoupled first and second bending modes and first torsion mode as used in the modified strip analysis. Figure 16 shows the calculated flutter-speed coefficients to be in good agreement with experimental values up to about M = 0.85. Above that Mach number, there are no subsonic experimental data for the 3-percent-thick wings, but the calculations are about 25 percent higher than data for the 4-percent-thick wings at M = 0.95.

Close agreement throughout the Mach number range is indicated between the kernel-function flutter speeds and the values obtained from the modified strip analysis. The largest difference between them is about 5 percent at M = 0. Similar comparisons for a wing with an aspect ratio of 4.0, a sweepback of 45°, and a taper ratio of 0.6 have shown kernel-function flutter speed at M = 0 to be about 10 percent higher than the value obtained by the modified strip analysis.

Model 2A-left.- Calculations for model 2A-left employed the first three coupled modes calculated by a matrix-iteration method as indicated in appendix A. The resulting flutter-speed coefficients shown in figure 16 are in good agreement with experimental values for Mach numbers up to 0.96. The kernel-function flutter speeds for model 2A-left, however, are somewhat lower than values for model 4A-right (uncoupled modes) throughout the Mach number range with the greatest difference occurring at the higher Mach numbers. Figure 17 shows little difference between the kernel-function flutter-frequency ratios for models 2A-left and 4A-right, except at the highest Mach numbers.

Piston Theory and Quasi-Steady Second-Order Theory

All the flutter speeds calculated for model B by piston theory and by quasi-steady second-order theory $\left(\text{air forces essentially proportional to } \dfrac{1}{M} \text{ and to } \dfrac{1}{\sqrt{M^2 - 1}}, \text{ respectively}\right)$ are higher than the experimental values. (See fig. 18(a).)
However, both the speeds and the frequencies (fig. 18) obtained by use of uncoupled modes are considerably closer to experimental values than are those obtained with coupled modes. These results are in contrast with the subsonic-kernel-function calculations for models 4A-right and 2A-left (figs. 16 and 17) in which relatively little difference appeared between coupled-mode and uncoupled-mode flutter speeds and frequencies. Figure 18(a) shows that flutter speeds obtained from quasi-steady second-order theory are lower and closer to experimental values than are those obtained from piston theory, although there is little difference between the corresponding flutter frequencies. (See fig. 18(b).) Also, use of the steady-state tip correction described previously yields lower flutter speeds and improves the comparison with experiment.

Best results with regard to both flutter speeds and frequencies were obtained from the uncoupled-mode second-order-theory analysis employing the steady-state tip correction. However, at a Mach number of 2.0, the resulting flutter speed is still about 38 percent higher than experiment. At least part of this deviation is attributed to the relatively low Mach number combined with the moderately high sweepback of the leading edge. At $M = 2.0$, the Mach number component normal to the leading edge is only 1.30. At higher Mach numbers, both piston theory and quasi-steady second-order theory would be expected to yield more accurate results. The round leading edge of this wing gives rise to a region of subsonic flow which probably also contributes to the discrepancy in the calculated flutter speeds. Such regions of embedded subsonic flow are not accurately represented by piston theory and second-order theory as employed herein.

For each of the piston-theory and second-order-theory calculations shown in figure 18, only single flutter solutions occurred so that the question of double flutter boundaries did not arise. However, a second-order-theory calculation at $M = 2.0$ employing uncoupled modes and the steady-state tip correction but neglecting finite wing thickness yielded no flutter solution. This result again points out the importance of including wing thickness in flutter analyses at the higher supersonic Mach numbers. The effects of finite wing thickness were previously indicated in connection with the modified-strip-theory calculations of figures 14 and 15.

CONCLUSIONS

The flutter characteristics of a highly tapered swept-wing planform have been investigated analytically by several methods. The results have been compared with experimental flutter data for Mach numbers up to 2.0. The following

conclusions are indicated with regard to the flutter frequency and the flutter-speed coefficient, which is the flutter speed divided by the streamwise root semichord, by the frequency of the first uncoupled torsion mode, and by the square root of the mass ratio:

1. Flutter speeds calculated by the modified-strip-analysis method of NACA RM L57L10 are in good agreement with experimental values at subsonic and low supersonic Mach numbers. An abrupt increase in flutter-speed coefficient with increasing Mach number, observed experimentally in the transonic range, is also indicated by the calculations.

2. In the supersonic range, some of the modified-strip-theory calculations yield two flutter speeds which are very close together. Under some conditions of density and Mach number, these two solutions indicate a discontinuous change of flutter frequency. An abrupt increase of flutter frequency in the transonic range has previously been observed experimentally.

3. Differences in flutter-speed-coefficient levels obtained from tests at low supersonic Mach numbers in two wind tunnels are also predicted by the modified strip theory. These differences are attributable primarily to differences in mass ratio for the two sets of tests.

4. At the higher Mach numbers (supersonic leading edge), use in the modified strip analysis of aerodynamic parameters obtained from linearized aerodynamic theory yields excessively high flutter speeds. However, use of aerodynamic parameters based on the Busemann second-order theory, which includes effects of finite wing thickness, gives an accurate prediction of flutter speed.

5. Flutter-speed coefficients calculated by the subsonic-kernel-function method are in good agreement with experimental values and with calculations made by the modified-strip-analysis method. Little difference appears between coupled-mode and uncoupled-mode flutter speeds except at the highest subsonic Mach numbers.

6. Flutter calculations were made for the higher supersonic Mach numbers by piston theory and by quasi-steady second-order theory, both with and without tip corrections and with coupled and uncoupled vibration modes. The results for the second-order theory with uncoupled modes and with an aerodynamic correction for the finite wing tip are closest to experimental flutter speeds and frequencies. These calculated flutter speeds, however, are about 38 percent higher than the experimental values.

Langley Research Center,
National Aeronautics and Space Administration,
Langley Station, Hampton, Va., December 3, 1962.

APPENDIX A

DETAILS OF WING DESCRIPTION

General

As mentioned previously, all wing panels analyzed in this investigation represented wings with a full-span aspect ratio of 4.0, a full-wing taper ratio of 0.2, a quarter-chord sweepback of 45°, and NACA 65A-series airfoil sections streamwise. All were of essentially homogeneous construction except those with added ballast along the leading edge. (See ref. 2.)

Wings tested in Langley transonic blowdown tunnel.- All of the wings tested in the Langley transonic blowdown tunnel (refs. 1 and 2) were full span and were cantilever mounted in the midwing position on a stationary cylindrical sting fuselage with diameter equal to 21.9-percent span. Models 1-left, 4A-right, and 2A-left of reference 1 were employed, as were models ballast I and ballast II of reference 2. All of these wings had NACA 65A003 airfoil sections streamwise, except model 1-left which had NACA 65A004 airfoil sections, also streamwise. The wing designated ballast I had an added mass equal to 6.25 percent of the basic wing mass distributed along the leading edge between $\bar{y} = 0.75$ and $\bar{y} = 1.00$. The wing designated ballast II had an added mass equal to 6.50 percent of the basic wing mass distributed along the leading edge between $\bar{y} = 0.50$ and $\bar{y} = 0.75$.

Wing tested in Langley supersonic aeroelasticity tunnel.- The wing tested in the Langley 9- by 18-inch supersonic aeroelasticity tunnel (results unpublished) was a semispan model which was cantilever mounted on the tunnel wall with no simulated fuselage. This wing had NACA 65A004 airfoil section streamwise and is designated model B.

Model Properties

Mode shapes and frequencies.- Uncoupled bending and torsional mode shapes for models 1-left, 4A-right, B, ballast I, and ballast II were calculated by the method of reference 13. The resulting first three bending mode shapes and first torsion mode shape for model 1-left are given in figure 22. Mode shapes for models 4A-right and B are generally similar to those for model 1-left and are not shown. The first two bending mode shapes and the first torsion mode shape for ballast I and ballast II are given in figures 23 and 24, respectively.

Modal frequencies used for the uncoupled modes were obtained from measured coupled mode frequencies. Following the procedure of reference 1, measured frequencies for coupled bending modes were used directly as uncoupled bending mode frequencies. Measured coupled torsion mode frequencies were "uncoupled" by means of the relation used in reference 1. It may be seen from node-line positions given in references 1 and 2 that the natural modes for these models are

not highly coupled, although some camber appears in the higher modes. Frequencies for both coupled and uncoupled modes are listed in table II.

Some of the flutter calculations of this investigation employed coupled vibration modes. The required first three coupled mode shapes and frequencies for model 2A-left were calculated by a matrix-iteration method which employed measured structural-influence coefficients and mass distribution. The resulting mode shapes are shown in figure 4, and the corresponding frequencies are compared with measured values in table II. The calculated frequencies for the first three modes are seen to differ from measured values by no more than 6 percent. Table II also shows that although models 2A-left and 4A-right were intended to be identical, model 2A-left appears to have been slightly weaker than model 4A-right.

For model B, coupled mode shapes and frequencies were measured. The measured shapes for model B shown in figure 5 are generally similar to the calculated mode shapes for model 2A-left (fig. 4) except that considerably more camber appears in the higher modes for model 2A-left than for model B. This situation would be expected since model 2A-left is thinner than model B. It should also be noted that the coupled mode shapes for model B (fig. 5) have been normalized with respect to maximum modal deflection, whereas the mode shapes for model 2A-left (fig. 4) have been normalized with respect to deflection at the tip quarter chord.

Mass and stiffness properties.- Model properties other than the mode shapes and frequencies just discussed were obtained from table I of reference 1 for models 1-left and 4A-right and from table II of reference 2 for ballast I and ballast II. For model B, the required distributions along the wing of elastic-axis position, local center of gravity, and local radius of gyration were not available. These quantities were therefore obtained from corresponding distributions for model 1-left by extrapolating the values inboard from the wing root to the model center line. These extrapolations were required because model 1-left had a fuselage, whereas model B did not. The two models should otherwise have been directly comparable. The extrapolations are considered to introduce insignificant errors into the flutter results because amplitudes of motion near the root of a cantilever wing are small so that values of quantities in that region are not heavily weighted in the flutter solution. Distributions of elastic-axis position, local center of gravity, and local radius of gyration were not needed for model 2A-left because only coupled mode flutter calculations were made for that wing.

APPENDIX B

PRELIMINARY FLUTTER ANALYSIS BY THE MODIFIED STRIP METHOD

Calculations

Preliminary flutter calculations for model 1-left were made by the modified strip method as described in reference 4; that is, the required distributions of steady-flow aerodynamic parameters were calculated for subsonic speeds by the lifting-line method of reference 17 and for supersonic speeds by the linearized lifting-surface method of reference 11 (when the leading edge was subsonic) or reference 12 (when the leading edge was supersonic). The aerodynamic parameters required for wing sections normal to the elastic axis were obtained from values for streamwise sections by application of simple sweep theory. Although this procedure proved satisfactory for the untapered and moderately tapered wings of reference 4, it was considered to be questionable for the highly tapered planform of the present report. Accordingly, for the final flutter calculations discussed in the body of this report, the aerodynamic parameters required were obtained by direct integration of lifting pressures along wing sections perpendicular to the elastic axis. In connection with this modification, figure 2 shows that for supersonic speeds, values of $c_{l_{\alpha,n}}$ obtained by use of simple sweep theory are in very good agreement with values obtained by direct integration. However, simple sweep theory yields aerodynamic-center positions $a_{c,n}$ that are too far forward at supersonic speeds. Also, to provide more accurate determination of the section lift-curve slopes and especially the local aerodynamic centers, the aerodynamic parameters used in the final calculations for subsonic speeds were computed from subsonic lifting-surface theory, essentially that of reference 10. For subsonic Mach numbers, values of $c_{l_{\alpha,n}}$ (fig. 2) obtained from the lifting-line theory of reference 17 are in satisfactory agreement with those obtained from lifting-surface theory, but the corresponding values of $a_{c,n}$ show appreciable differences near the wing tip. These differences however, would not be expected to cause large differences in the resulting subsonic flutter characteristics. As shown in reference 14, subsonic flutter characteristics are generally not very sensitive to changes in local aerodynamic-center position. As a result of the preceding comparisons, the aerodynamic parameters used in all subsequent calculations were obtained from lifting-surface theory by direct integration of lifting pressure. As illustrated in reference 15, transonic flutter characteristics may be calculated by the modified strip method if the aerodynamic parameters are obtained from measured transonic pressure distributions. However, such data were not available for the wing of this investigation, so that continuous distributions of flutter characteristics through the transonic range could not be calculated.

Most of the modified-strip-theory calculations in this report employed the calculated uncoupled first torsion mode and first and second bending modes. However, a few of the preliminary calculations included the third bending mode for comparison. Also, for comparison, some of the preliminary calculations used the first torsion mode and the first and second bending modes of a uniform cantilever

beam. As indicated previously, the uncoupled modal frequencies employed were obtained from measured frequencies and are listed in table II.

Results

The results of the preliminary flutter calculations are shown in figures 25 to 27. The flutter speeds are compared in figure 25 in the form of the flutter-speed coefficient $\dfrac{V}{b_s \omega_\alpha \sqrt{\mu}}$ and in figure 26 in the form of flutter-speed ratio $\dfrac{V}{V_R}$. In the latter comparison, the normalizing reference flutter speed V_R for each theoretical or experimental point was calculated by the modified strip method with the density associated with the numerator V and with aerodynamic parameters for two-dimensional incompressible flow $\left(c_{l_{\alpha,n}} = 2\pi \text{ and } a_{c,n} = -\dfrac{1}{2}\right)$. The mode shapes and frequencies used in the V_R calculations were the same as for the numerator V. Values of V_R for the experimental points were calculated by use of calculated first torsion and first and second bending modes.

Both the flutter-speed-coefficient and flutter-speed-ratio forms of data presentation are employed because each has specific advantages which should not be obscured by the fact that the resulting curves are generally similar in shape. For example, the flutter-speed coefficient is, for a given wing, proportional to the square root of the flutter dynamic pressure. This form of presentation is therefore useful for illustrating changes in the dynamic pressure caused, for instance, by changes in flow density. The flutter-speed ratio, on the other hand, is useful in examining results especially for the modified strip analysis, because this ratio tends to isolate aerodynamic effects. That is, the normalizing reference flutter speed V_R is calculated from the same input quantities as the numerator V, except that two-dimensional incompressible-flow aerodynamic parameters are used for V_R. Thus, the flutter-speed ratio conveniently reflects the effects of finite planform and nonzero Mach number. As a matter of further interest, the flutter speeds presented in figures 6, 8, and 16 are also shown in figures 28 to 30 in the form of $\dfrac{V}{V_R}$.

The preliminary flutter calculations shown in figures 25 to 27 were made for model 1-left only. This 4-percent-thick wing was initially chosen for this analysis because it was thought that camber deflections would be less evident in the vibration modes for a 4-percent-thick wing than in the modes for a 3-percent-thick wing. (Compare figs. 4 and 5.) The use of uncoupled beam-type modes (required for the modified strip analysis as presently formulated) should therefore be more appropriate for the thicker wing. The density $\rho = 0.0060$ slug/cu ft used in all of the calculations shown in figures 25 to 27 was chosen as representative of the values for the highest Mach numbers at which experimental flutter points were obtained for model 1-left.

The four-mode calculations in figures 25 and 27 show that even for the highly tapered planform of this investigation, the use of simple sweep theory for the evaluation of aerodynamic parameters yields reasonably accurate flutter results in the subsonic range. At supersonic Mach numbers, however, the more accurate evaluation of aerodynamic parameters by direct integration of lifting pressure (fig. 2) gives appreciably better results than simple sweep theory.

Figures 25 and 27 also indicate that inclusion of the fourth mode (third bending) in the flutter analysis does not significantly affect the results. Even use of uniform-beam modes does not appreciably alter flutter speeds at subsonic Mach numbers. Figure 25 does indicate, though, that use of accurate modes becomes more important at supersonic speeds. In accordance with these results, the fourth mode was not included in any subsequent calculations.

The flutter-speed values shown in figure 25 are replotted in figure 26 as flutter-speed ratio $\frac{V}{V_R}$. The relative levels of the calculated curves and the experimental points in figure 26 appear to be different from those of figure 25. Moreover, the relative levels of the calculated curves themselves are different, most notably at subsonic speeds. These differences arise for two reasons. First, the values of V_R for the various calculated curves are different because of the different types and numbers of modes employed. Second, the effect of density is taken into account differently in the two presentations. In the flutter-speed coefficient $\frac{V}{b_s \omega_\alpha \sqrt{\bar{\mu}}}$ the flutter speed is divided by a parameter which is inversely proportional to the square root of density, whereas the value of V_R is related to density in a more complicated way. (See ref. 14.) Although all of the calculated curves of figures 25 and 26 are associated with the same density ($\rho = 0.0060$ slug/cu ft or $\bar{\mu} = 14.96$), the experimental points and their normalizing V_R values were obtained at varying density. Hence, the density differences between theoretical and experimental points are accounted for differently in the two figures.

The fact that the calculated subsonic flutter speeds and frequencies in figures 25 to 27 are higher than the experimental points is attributed, at least in part, to the fact that the density used in the preliminary calculations ($\rho = 0.0060$ slug/cu ft) was appreciably higher than the values associated with the experimental subsonic flutter points. Reference 14 showed that both flutter-speed ratio $\frac{V}{V_R}$ and flutter-frequency ratio $\frac{\omega}{\omega_\alpha}$ increase as density increases. Therefore, in order to represent experimental conditions more accurately, all final subsonic flutter calculations employ a representative density for the experimental subsonic flutter points, and all final supersonic flutter calculations use a representative density for the experimental supersonic points.

The comparisons of figures 25 and 26, together with the foregoing discussion, emphasize the need for caution in choosing a form for presenting flutter data and in choosing the density (or mass ratio) for use in theoretical analyses. It

may not be sufficient simply to attempt to correlate results at different densities on the basis of some combination parameter, such as the flutter-speed coefficient $\dfrac{V}{b_s \omega_\alpha \sqrt{\mu}}$.

APPENDIX C

EFFECTS ON FLUTTER DATA OF WIND-TUNNEL OPERATING CONDITIONS AND WING SIZE

Comparison of Flutter Conditions for a Given Wing

in the Atmosphere and in a Wind Tunnel

As mentioned earlier in this report, the track traced across the flutter-speed surface for a given wing (fig. 21, for example) by flutter speeds measured in a particular wind tunnel may be different from that traced out in another tunnel or in the atmosphere. Such differences may result, for example, from differences in static-temperature level, particularly in blowdown wind tunnels. As an illustration, consider the Langley transonic blowdown tunnel, in which the data of references 1 and 2 were obtained. Mach number and air density may be varied independently in this tunnel, but during a run, the static temperature in the test section may drop from ambient atmospheric temperature to 410° R or lower.

For this example consider the flutter conditions for model 4A-right at a Mach number of 1.30 in standard atmosphere and in the Langley transonic blowdown tunnel. Figure 31 shows a cross section of the calculated flutter-speed surface for this wing at $M = 1.30$. Flutter for model 4A-right at this Mach number in standard atmosphere would correspond to point F_a in figure 31, for which $\bar{\mu}_a = 27.87$. If the values $\bar{\mu}_a = 27.87$ and $M_a = 1.30$ are duplicated in the Langley transonic blowdown tunnel at a temperature $T_t = 448.1^\circ$ R, which is significantly less than $T_a = 530.2^\circ$ R, than the speed of sound and hence the free-stream velocity will be less than the corresponding values for flutter in standard atmosphere. The point attained in the tunnel then will be point t in figure 31, for which the velocity is

$$V_t = V_a \sqrt{\frac{T_t}{T_a}}$$

and the wing will not flutter. If then the Mach number M_a is maintained and the tunnel air density is increased, a path such as the dashed curve shown in figure 31 from points t to F_t will be followed until the wing flutters in the tunnel at point F_t. If the temperature T_t is constant during this operation,[1] the free-stream velocity V_t will remain constant. The flutter-speed coefficient associated with point F_t, however, will be greater than that for point F_a. Of course, the closer T_t is to T_a, the closer point t will be to point F_a, and hence the closer point F_t will be to point F_a with regard to both flutter-speed coefficient and mass ratio. Thus, if the tunnel temperature T_t were raised,

---

[1]During the operation of the Langley transonic blowdown tunnel, the test-section temperature changes continuously. However, for simplicity in the present discussion, the temporal aspects of the tunnel operation are ignored.

or if the temperature T_a associated with the flutter point F_a were lower, the points F_a and F_t would be closer together. However, if the desired mass ratio were increased above $\bar{\mu}_a$ (increasing altitude), the flutter-speed coefficient obtained in the tunnel, point F_t, would become increasingly unconservative with respect to point F_a, particularly at the higher Mach numbers.

In the preceding discussion the influence of viscosity has not been mentioned. Certainly changes in the wing boundary layer with changing Reynolds number could affect the onset of flutter. Possibly more important, though, is the level of turbulence in the tunnel. Turbulence would be expected to act as a driving force for the wing and hence lower the observed flutter boundary.

In the present illustration the dynamic pressure associated with point F_t is about 14 percent greater than that for point F_a. This difference could be even larger, of course, if the comparison were made for a density corresponding to an altitude greater than sea level $\left(\bar{\mu}_a > \bar{\mu}_{sea\ level}\right)$. For instance, some airplanes currently operate at mass ratios near 50.

It should be remembered that this example refers to flutter conditions in the atmosphere and in a wind tunnel for a given wing. In general, it does not apply to model-prototype comparisons in which flutter conditions for the prototype in the atmosphere are derived from wind-tunnel tests of a model scaled to represent the prototype near a $\bar{\mu},M$ point at which flutter was obtained in the tunnel. The discussion would apply, however, for scaled flutter models which are tested at off-design mass ratios.

Effects of Wing Size[2]

Flutter analyses (e.g., this report and ref. 14) indicate that the flutter speed and frequency of a given wing are primarily functions of the air density (or mass ratio) and the Mach number. If values are specified for the independent variables $\bar{\mu}$ and M, other pertinent quantities are automatically determined, as is illustrated in the following table:

Independent variable	Principal dependent variable	Related dependent variable
Mach number	Flutter speed	Speed of sound
Mass ratio	Flutter frequency	$\begin{cases} \text{Temperature} \\ \text{Reduced frequency} \end{cases}$

---

[2]This discussion is not intended to be a treatise on model scaling, because only a limited class of wings is discussed. The implications of dissimilar models, weakened models, or models with internal structure different from prototype are not considered. A more general discussion of model scaling may be found, for example, in reference 18.

More specifically, for a given wing,

$$\frac{V}{b_s \omega_\alpha \sqrt{\bar{\mu}}} = f_1(\bar{\mu}, M) \tag{C1}$$

and

$$\frac{\omega}{\omega_\alpha} = f_2(\bar{\mu}, M) \tag{C2}$$
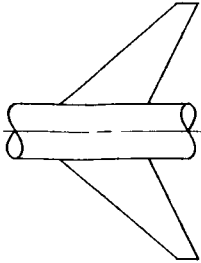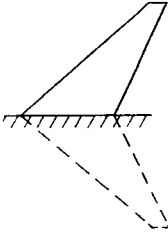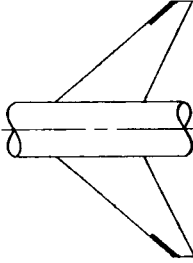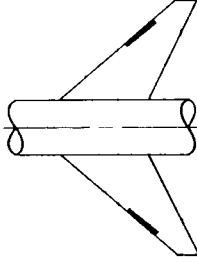
For wings of differing size that are geometrically similar and constructed of the same material (or of different materials for which the Young's modulus, the shear modulus, and the material density are proportional), the natural frequencies will be inversely proportional to the length scale. Also, equations (C1) and (C2) are independent of the length scale, so that the surfaces of flutter-speed coefficient and flutter-frequency ratio represented by these equations will be the same for all the wings of this type. Thus, for this particular class of wings the flutter speed as well as the flutter-speed coefficient will be independent of size. Further, inasmuch as equations (C1) and (C2) are independent of length scale, the reduced frequency is also independent of size. Finally, if the geometrically similar wings of different sizes are constructed of materials of the same density, then the flutter dynamic pressure will also be independent of length scale.

REFERENCES

1. Unangst, John R.: Transonic Flutter Characteristics of an Aspect-Ratio-4, 45° Sweptback, Taper-Ratio-0.2 Plan Form. NASA TM X-136, 1959.

2. Unangst, John R.: Transonic Flutter Characteristics of a 45° Sweptback Wing With Various Distributions of Ballast Along the Leading Edge. NASA TM X-135, 1959.

3. Stonesifer, John C., and Goetz, Robert C.: Transonic and Supersonic Flutter Trend Investigation of a Variable-Sweep Wing. NASA TM X-598, 1961.

4. Yates, E. Carson, Jr.: Calculation of Flutter Characteristics for Finite-Span Swept or Unswept Wings at Subsonic and Supersonic Speeds by a Modified Strip Analysis. NACA RM L57L10, 1958.

5. Watkins, Charles E., Woolston, Donald S., and Cunningham, Herbert J.: A Systematic Kernel Function Procedure for Determining Aerodynamic Forces on Oscillating or Steady Finite Wings at Subsonic Speeds. NASA TR R-48, 1959.

6. Lighthill, M. J.: Oscillating Airfoils at High Mach Number. Jour. Aero. Sci., vol. 20, no. 6, June 1953, pp. 402-406.

7. Ashley, Holt, and Zartarian, Garabed: Piston Theory - A New Aerodynamic Tool for the Aeroelastician. Jour. Aero. Sci., vol. 23, no. 12, Dec. 1956, pp. 1109-1118.

8. Morgan, Homer G., Huckel, Vera, and Runyan, Harry L.: Procedure for Calculating Flutter at High Supersonic Speed Including Camber Deflections, and Comparison With Experimental Results. NACA TN 4335, 1958.

9. Van Dyke, Milton D.: A Study of Second Order Supersonic Flow Theory. NACA Rep. 1081, 1952. (Supersedes NACA TN 2200.)

10. Falkner, V. M.: The Calculation of Aerodynamic Loading on Surfaces of Any Shape. R & M No. 1910, British A.R.C., Aug. 1943.

11. Cohen, Doris: Formulas for the Supersonic Loading, Lift, and Drag of Flat Swept-Back Wings With Leading Edges Behind the Mach Lines. NACA Rep. 1050, 1951.

12. Lagerstrom, P. A., Wall, D., and Graham, M. E.: Formulas in Three-Dimensional Wing Theory. Rep. No. SM-11901, Douglas Aircraft Co., Inc., July 8, 1946.

13. Houbolt, John C., and Anderson, Roger A.: Calculation of Uncoupled Modes and Frequencies in Bending or Torsion of Nonuniform Beams. NACA TN 1522, 1948.

14. Yates, E. Carson, Jr.: Some Effects of Variations in Density and Aerodynamic Parameters on the Calculated Flutter Characteristics of Finite-Span Swept and Unswept Wings at Subsonic and Supersonic Speeds. NASA TM X-182, 1960.

15. Yates, E. Carson, Jr.: Use of Experimental Steady-Flow Aerodynamic Parameters in the Calculation of Flutter Characteristics for Finite-Span Swept or Unswept Wings at Subsonic, Transonic, and Supersonic Speeds. NASA TM X-183, 1960.

16. Bisplinghoff, Raymond L., Ashley, Holt, and Halfman, Robert L.: Aeroelasticity. Addison-Wesley Pub. Co., Inc. (Cambridge, Mass.), c.1955.

17. DeYoung, John, and Harper, Charles W.: Theoretical Symmetric Span Loading at Subsonic Speeds for Wings Having Arbitrary Plan Form. NACA Rep. 921, 1948.

18. Head, A. L., Jr.: A Philosophy of Design for Flutter. Proc. Nat. Specialists Meeting on Dynamics and Aeroelasticity (Fort Worth, Texas), Inst. Aero. Sci., Nov. 1958, pp. 59-65.

TABLE I.- WINGS EMPLOYED IN FLUTTER ANALYSES

Model	Reference	Tunnel (a)	Exposed-panel aspect ratio (b)	Exposed-panel taper ratio (b)	NACA airfoil (streamwise)	Ballast mass, fraction of basic panel mass	Configuration
1-left 4A-right 2A-left	1 1 1	TBT TBT TBT	1.8291 1.8291 1.8291	0.2425 .2425 .2425	65A004 65A003 65A003	----- ----- -----	
B	Unpublished	SAT	2.0000	0.2000	65A004	-----	
Ballast I	2	TBT	1.8291	0.2425	65A003	0.0625	
Ballast II	2	TBT	1.8291	0.2425	65A003	0.0650	

[a] The designation TBT indicates the Langley transonic blowdown tunnel, and the designation SAT indicates the Langley 9- by 18-inch supersonic aeroelasticity tunnel.

[b] All models corresponded to a planform with full-wing aspect ratio of 4.0, full-wing taper ratio of 0.2, and quarter-chord sweepback angle of 45°.

TABLE II.- SUMMARY OF MODAL FREQUENCIES

Model	Source	Coupled mode frequencies				Uncoupled mode frequencies			
		ω_1	ω_2	ω_3	ω_4	$\omega_{h,1}$	$\omega_{h,2}$	$\omega_{h,3}$	ω_α (a)
1-left	Measurement	675	2,136	4,210	4,957	675	2,136	4,957	4,147
4A-right	Measurement	603	1,966	3,437	4,385	603	1,966	4,385	3,204
2A-left	Measurement	565	1,753	3,342	4,178	565	1,753	4,178	3,117
2A-left	Calculation	532	1,694	3,456	4,824	---	-----	-----	-----
B	Measurement	779	2,325	2,890	-----	779	2,325	-----	2,861
Ballast I	Measurement	466	1,665	2,663	3,631	466	1,665	3,631	2,652
Ballast II	Measurement	482	1,520	2,871	3,612	482	1,520	3,612	2,563

[a] The values of ω_α shown were obtained from the coupled torsion mode frequencies ω_3 by use of the "uncoupling" relation given in reference 1.

TABLE III.- INDEX TO FLUTTER CALCULATIONS

Model	Calculation method	Steady-flow aerodynamic theory[a]			Vibration modes			Results shown in figure —
		Subsonic	Supersonic	Air forces computed by—	Number	Type	Source	
1-left	Modified strip	Lifting surface	Lifting surface	Direct integration	4	Uncoupled	Calculation	25 to 27
	Modified strip	Lifting line	Lifting surface	Simple sweep theory	4	Uncoupled	Calculation	25 to 27
	Modified strip	Lifting line	Lifting surface	Simple sweep theory	3	Uncoupled	Calculation	25 to 27
	Modified strip	Lifting line	Lifting surface	Simple sweep theory	3	Uncoupled	Uniform beam	25 to 27
	Modified strip	Lifting surface	Lifting surface	Direct integration	3	Uncoupled	Calculation	6 to 9, 28, 29
4A-right	Modified strip	Lifting surface	Lifting surface	Direct integration	3	Uncoupled	Calculation	6 to 9, 14 to 17, 28 to 30
	Kernel function	---	---	---	3	Uncoupled	Calculation	16, 17, 30
2A-left	Kernel function	---	---	---	3	Coupled	Calculation	16, 17, 30
B	Modified strip	---	Lifting surface	Direct integration	3	Uncoupled	Calculation	14, 15
	Modified strip	---	Busemann second order	Direct integration	3	Uncoupled	Calculation	14, 15
	Piston theory	---	---	---	3	Uncoupled	Calculation	18
	Piston theory	---	---	---	3	Coupled	Measurement	18
	Second-order theory	---	---	---	3	Coupled	Measurement	18
	Second-order theory	---	---	---	3	Uncoupled	Calculation	18
Ballast I	Modified strip	Lifting surface	Lifting surface	Direct integration	3	Uncoupled	Calculation	10, 11
Ballast II	Modified strip	Lifting surface	Lifting surface	Direct integration	3	Uncoupled	Calculation	12, 13

a Aerodynamic parameters from steady-flow theory are required only in modified strip analysis.
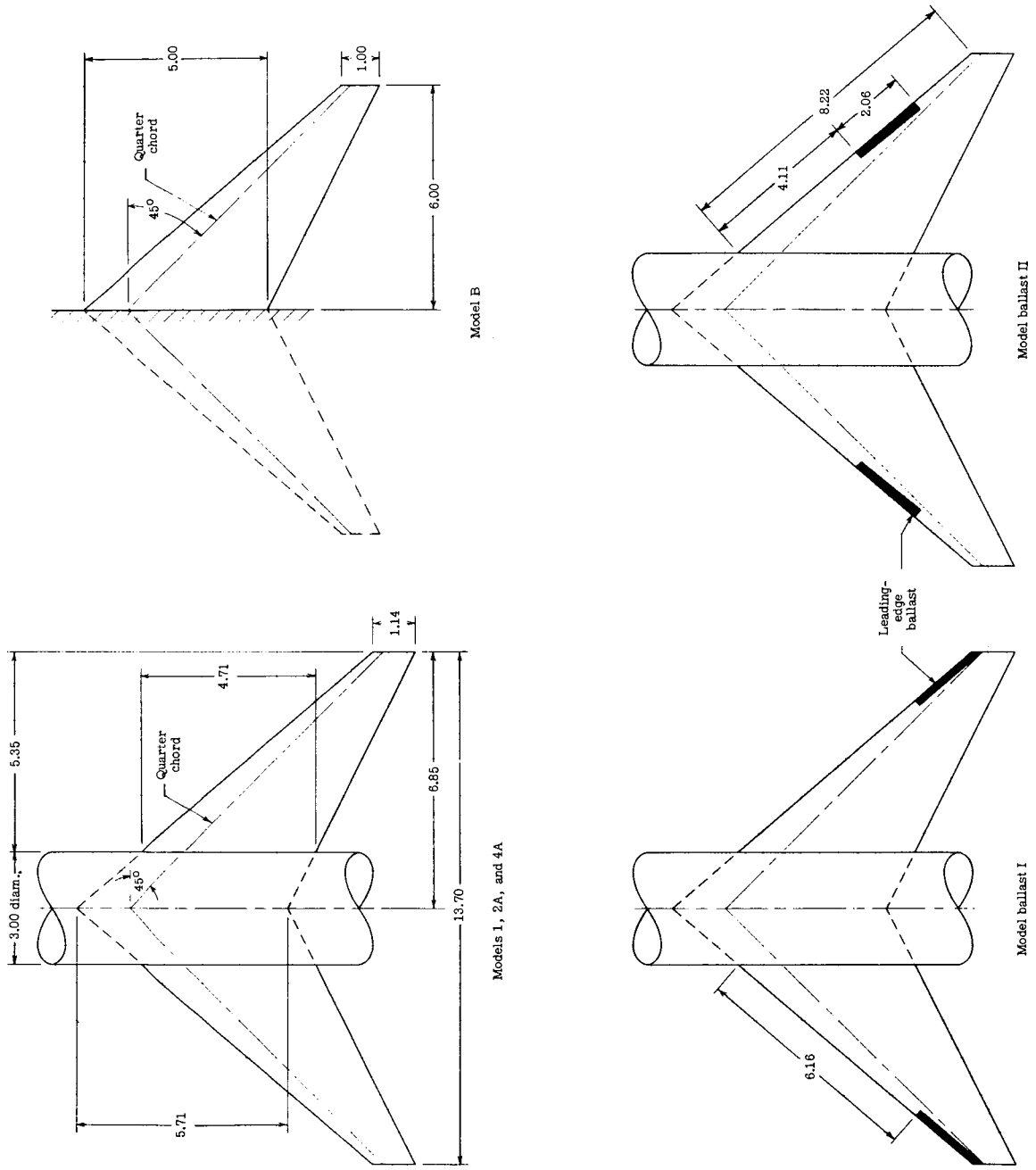
Figure 1.- Planforms of wings used in flutter analysis. All dimensions are in inches unless other-
wise noted. Dimensions for ballasted models are same as for model 1.
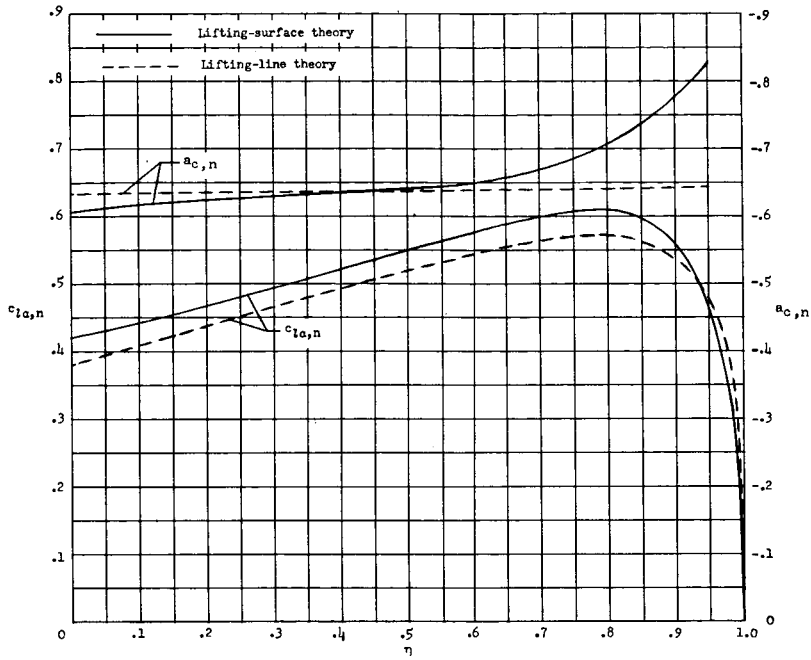
(a) M = 0.
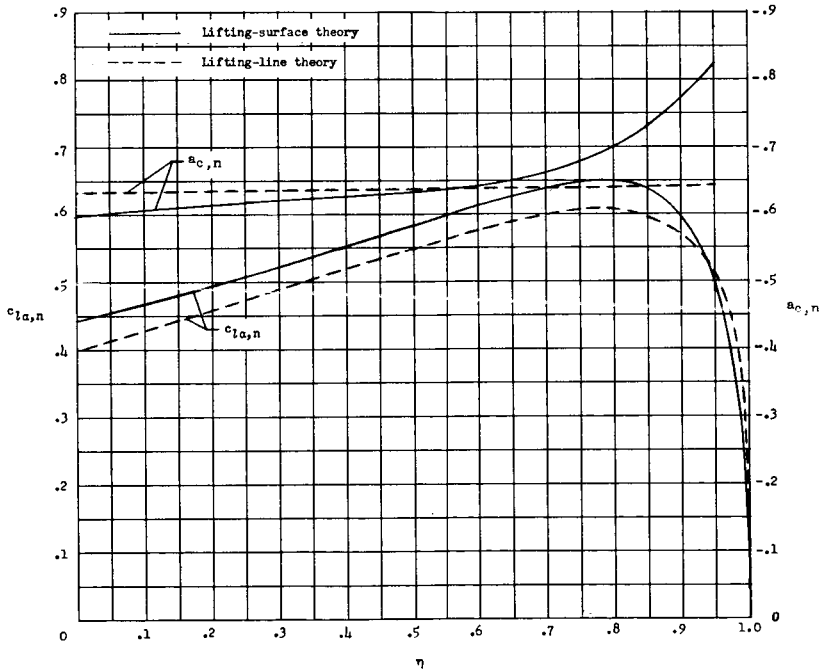
(b) M = 0.50.

Figure 2.- Distributions of steady-flow aerodynamic parameters calculated for model 1-left from linearized aerodynamic theories at several Mach numbers.
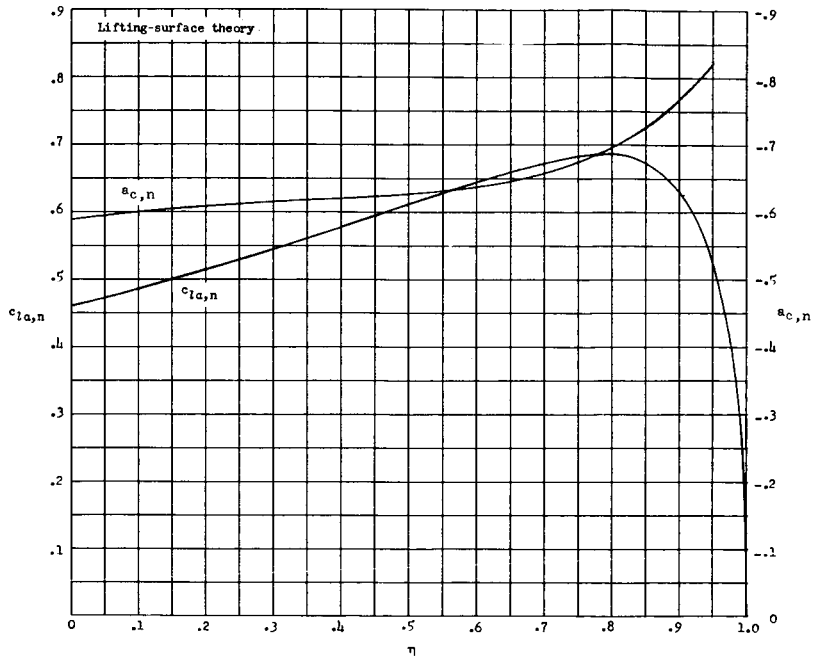
(c) M = 0.65.
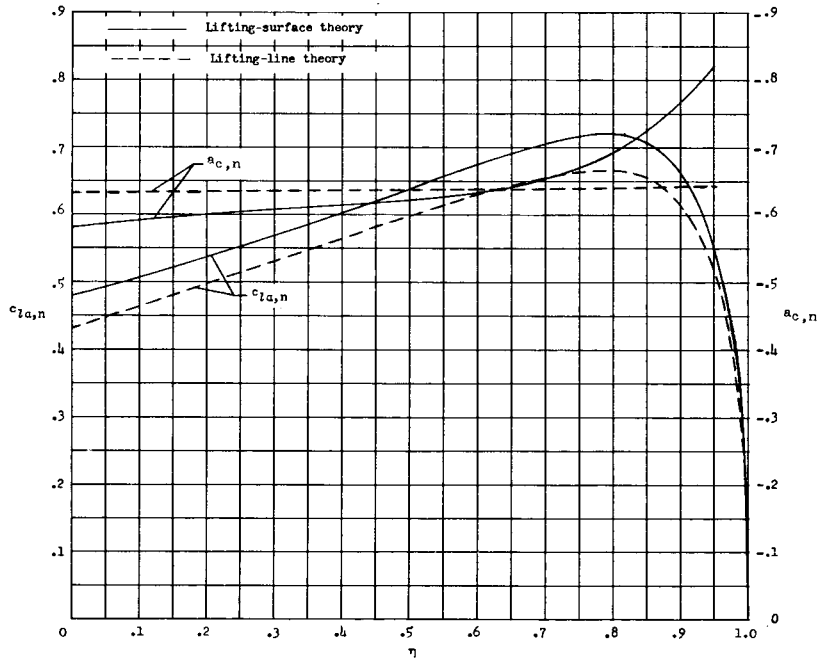
(d) M = 0.75.

Figure 2.- Continued.
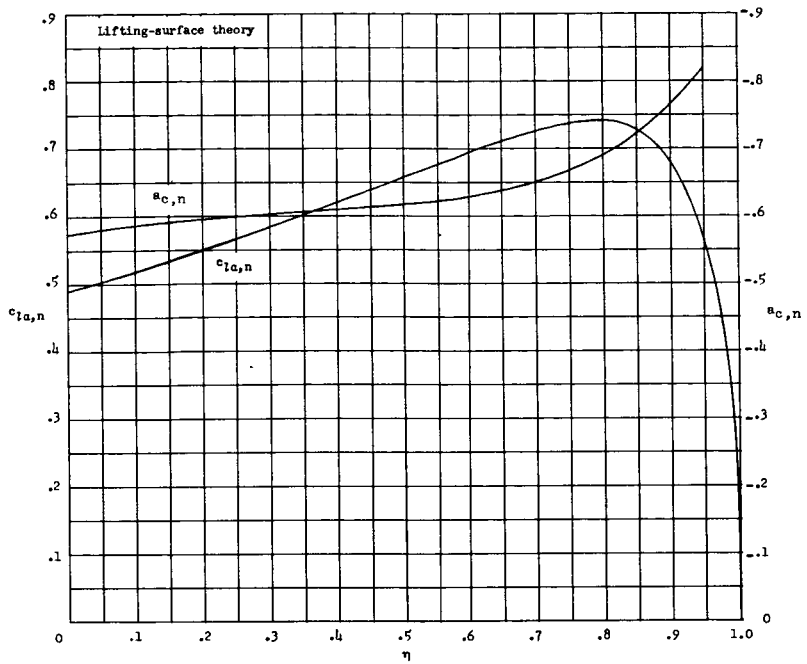
(e) M = 0.80.
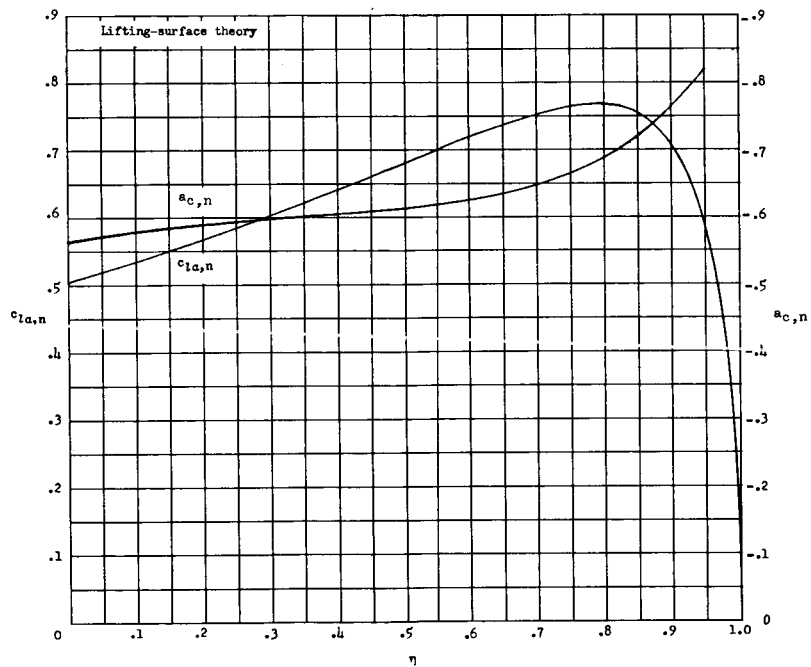
(f) M = 0.85.

Figure 2.- Continued.
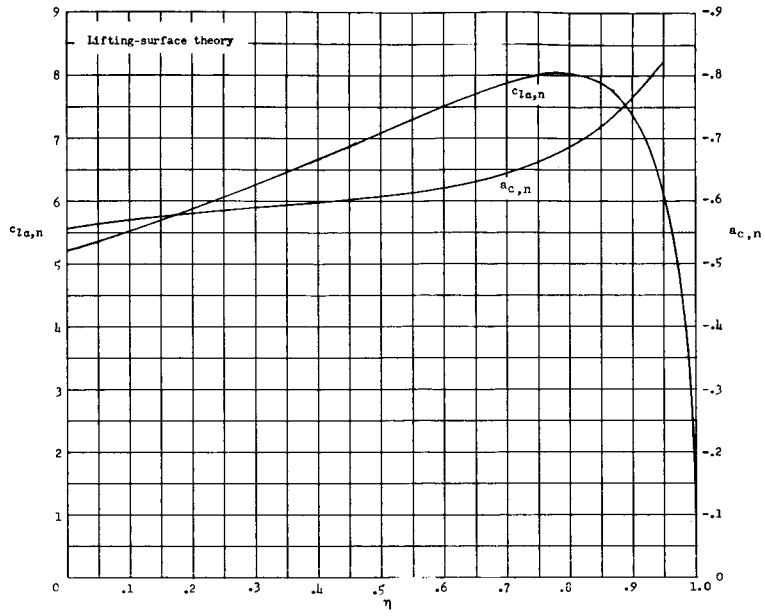
(g)   M = 0.90.
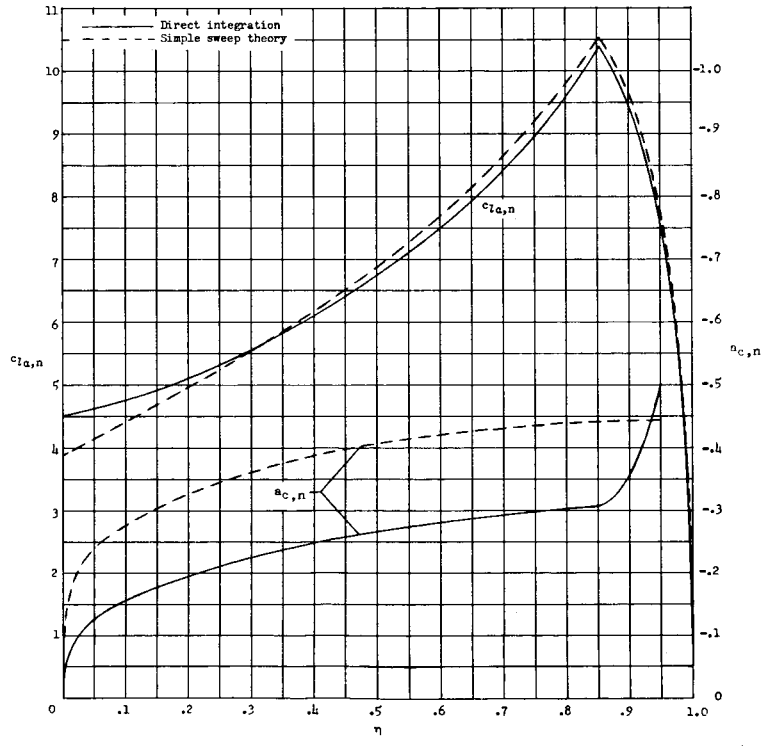
(h)   M = $2/\sqrt{3}$.

Figure 2.- Continued.
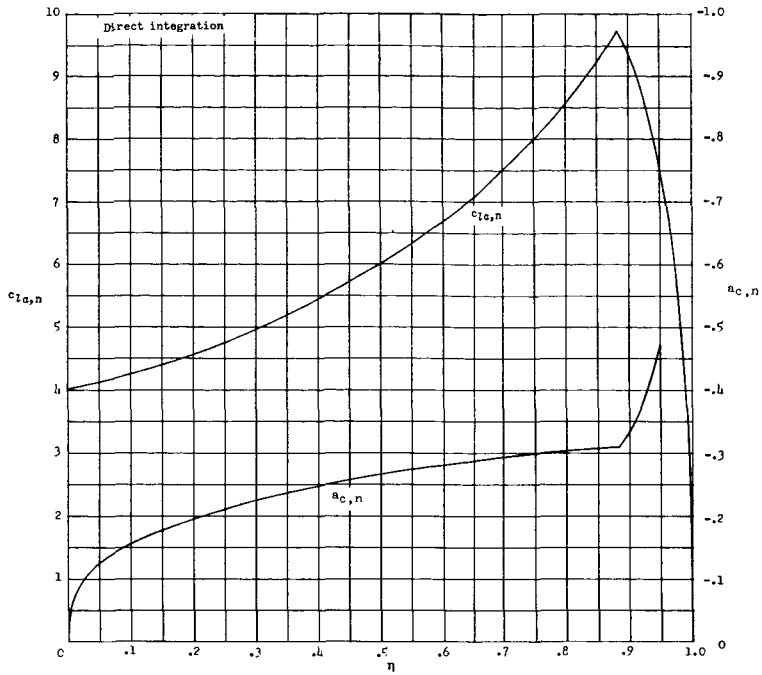
(i) M = 1.30.
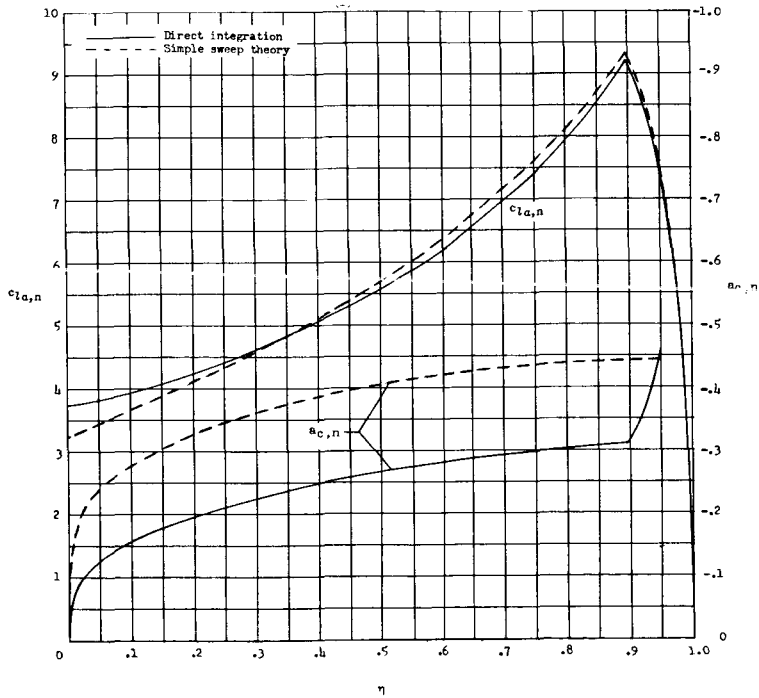
(j) M = $\sqrt{2}$.

Figure 2.- Concluded.
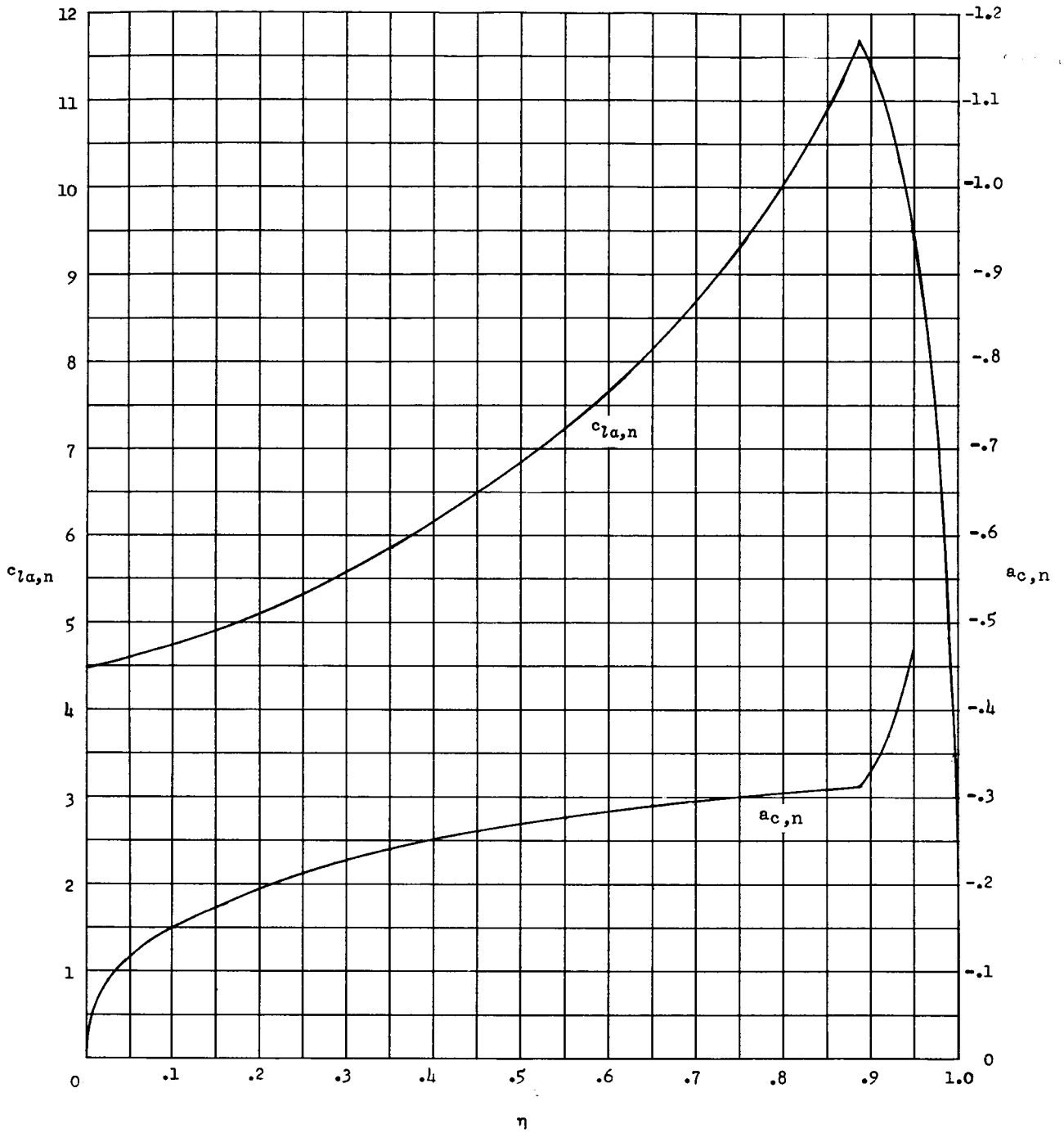
(a)   M = $2/\sqrt{3}$.

Figure 3.- Distributions of steady-flow aerodynamic parameters calculated by direct integration for model B at several Mach numbers. All values were obtained from linearized lifting-surface theory unless otherwise specified.
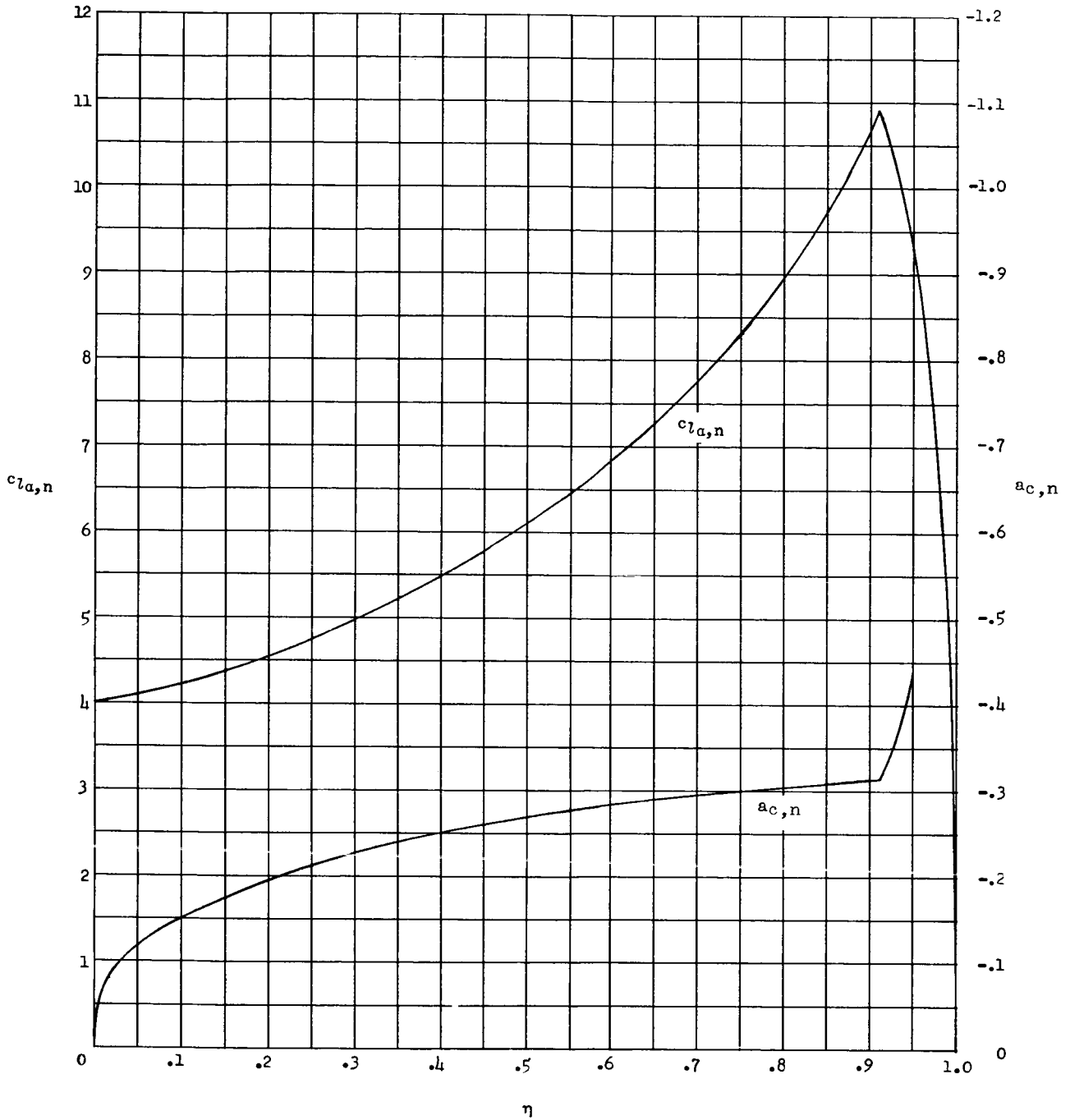
(b) M = 1.30.

Figure 3.- Continued.
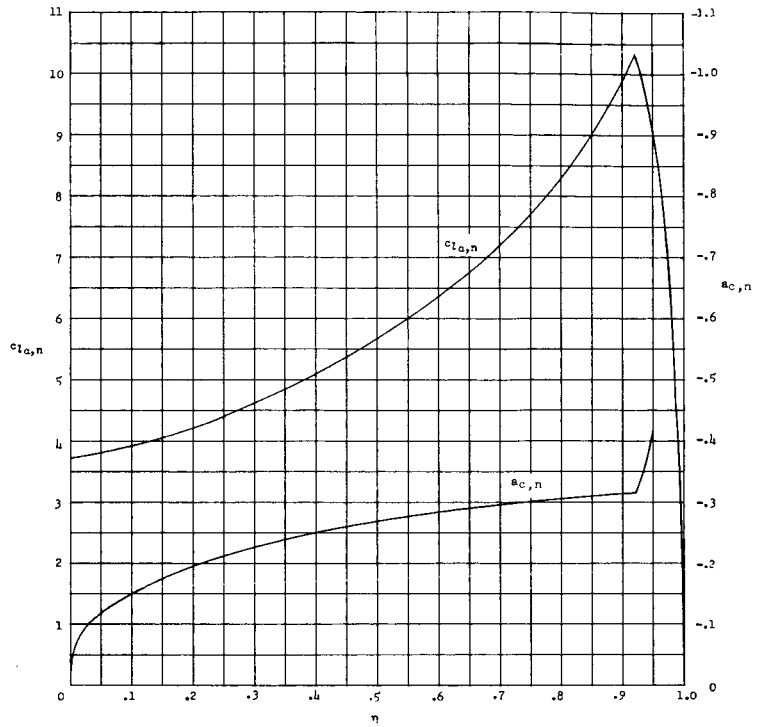
(c)   M = $\sqrt{2}$.
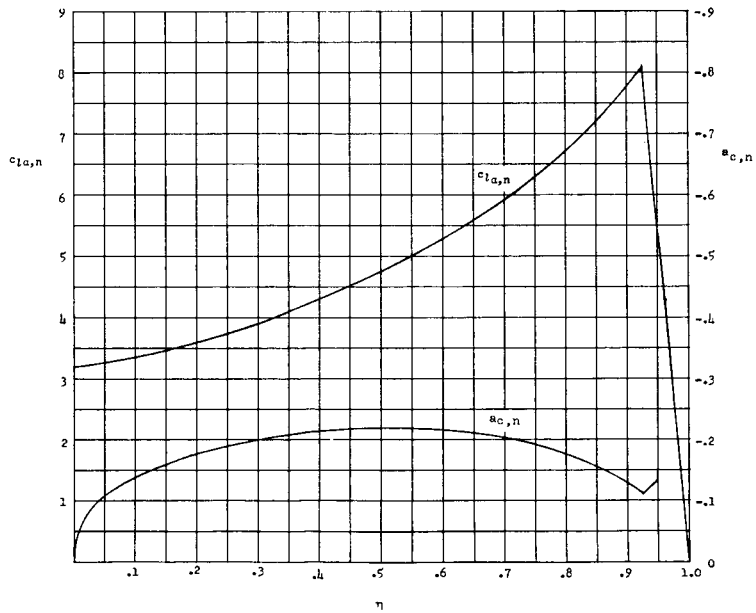
(d)   M = 1.64.

Figure 3.- Continued.
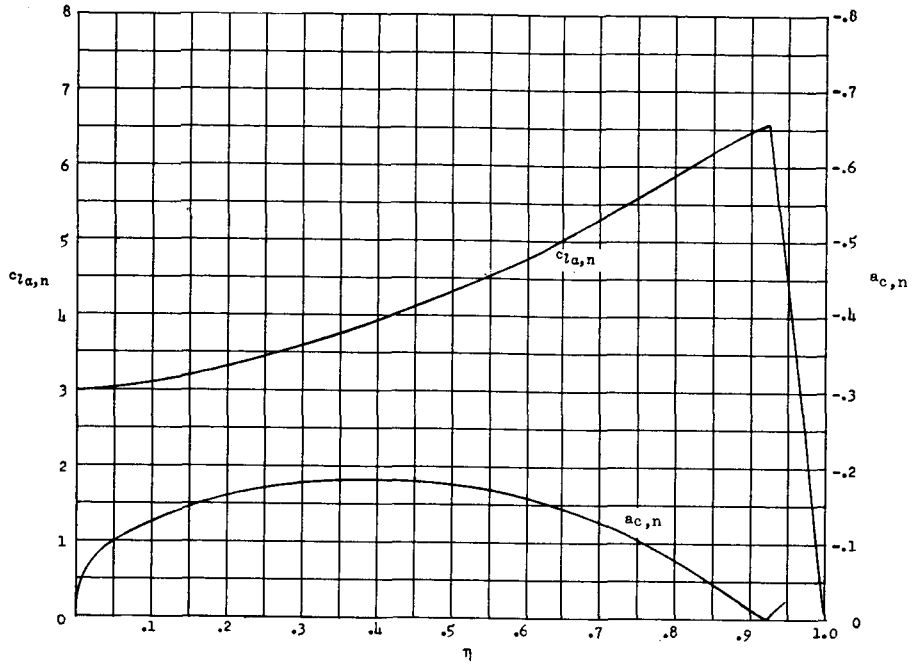
(e) M = 1.75.
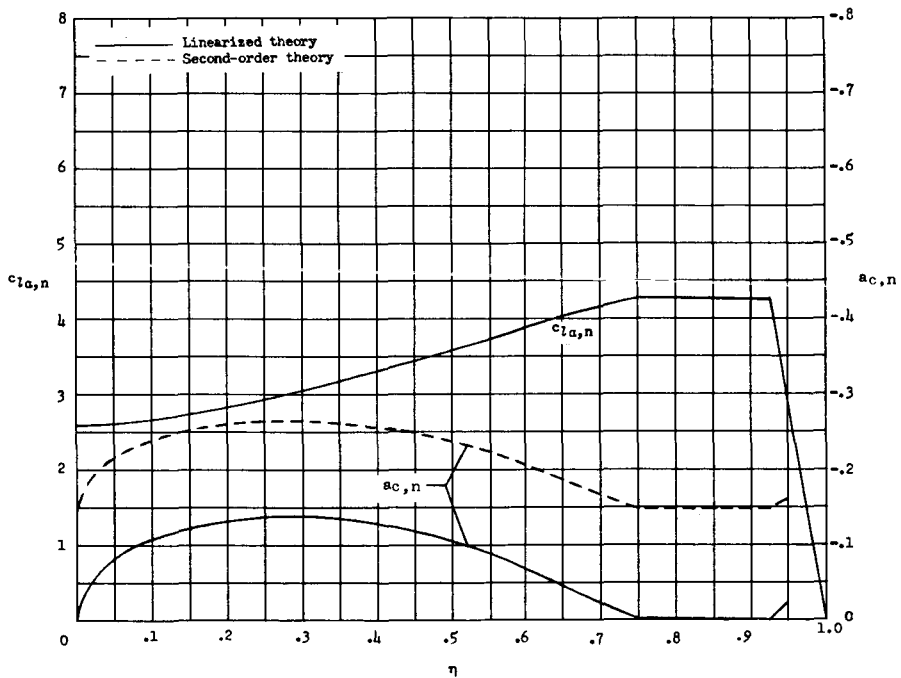
(f) M = 2.00.

Figure 3.- Concluded.
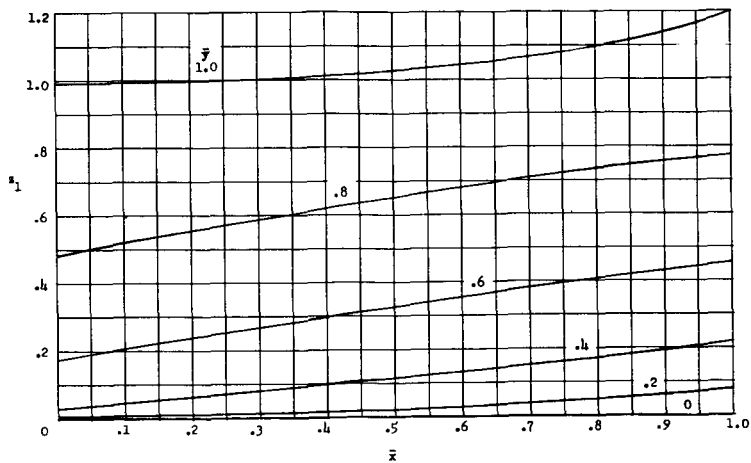
(a) First mode.
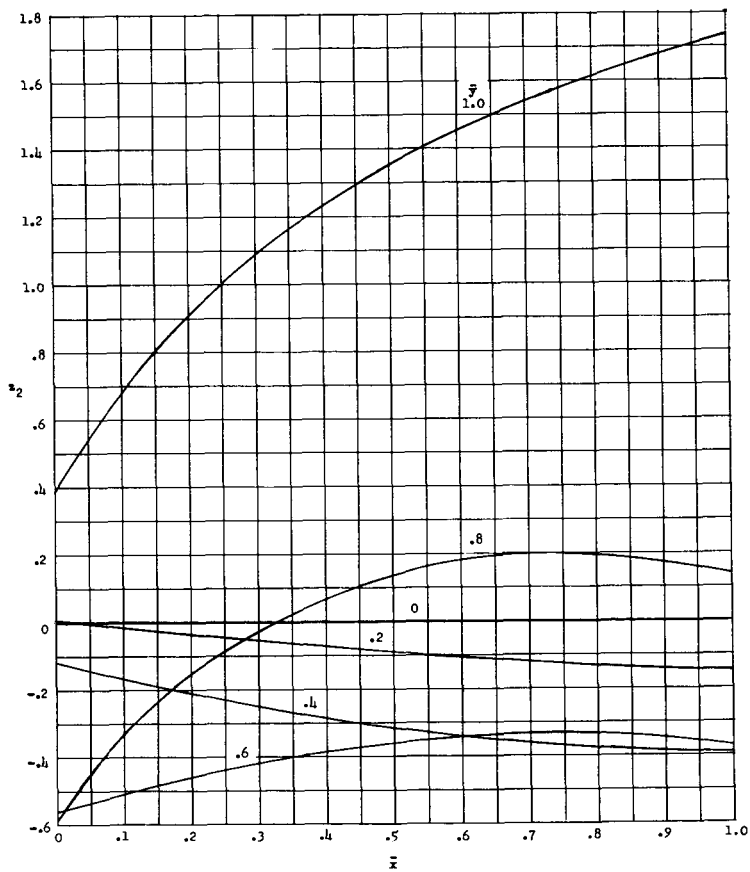
(b) Second mode.

Figure 4.- First three coupled vibration modes calculated for model 2A-left.
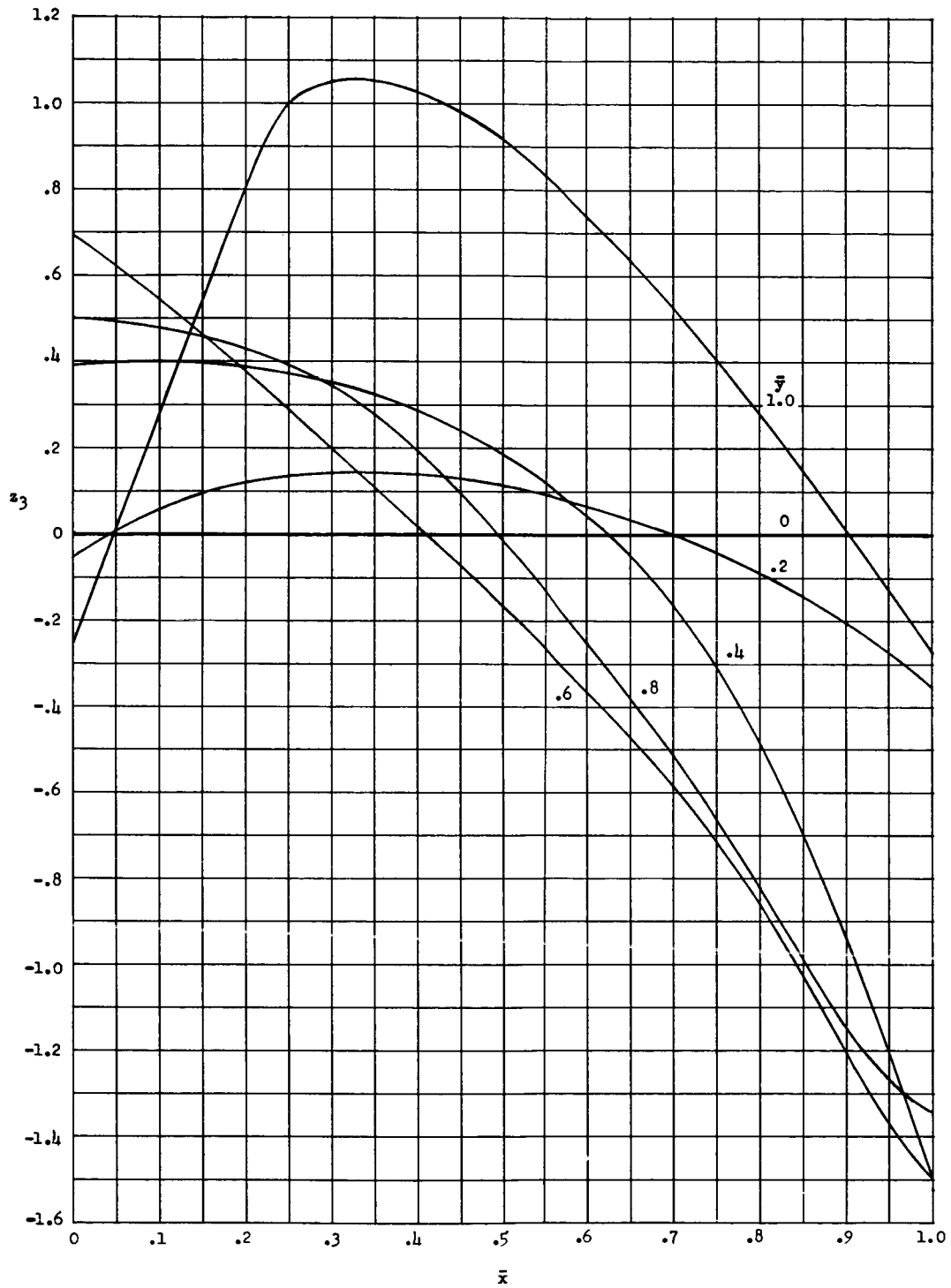
(c) Third mode.

Figure 4.- Concluded.
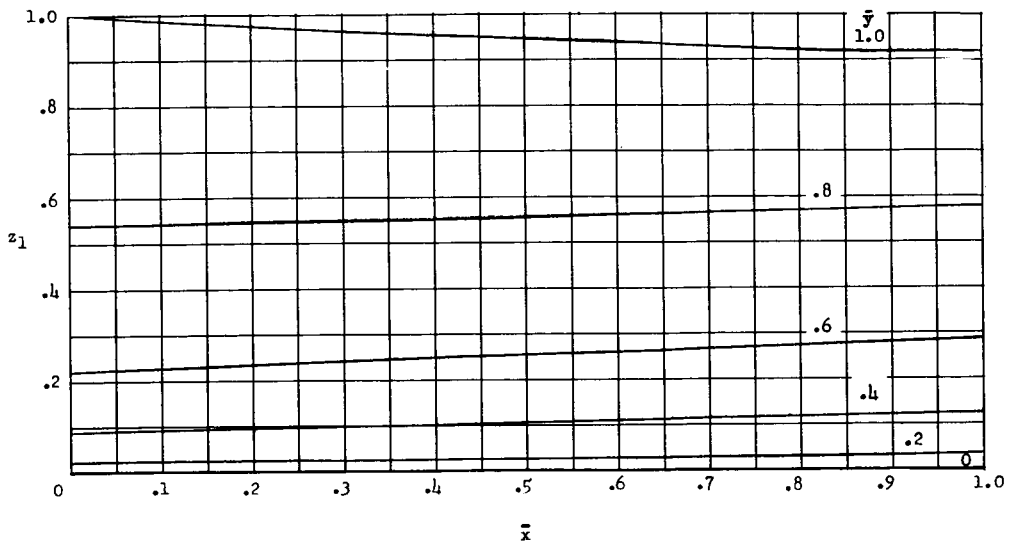
(a) First mode.
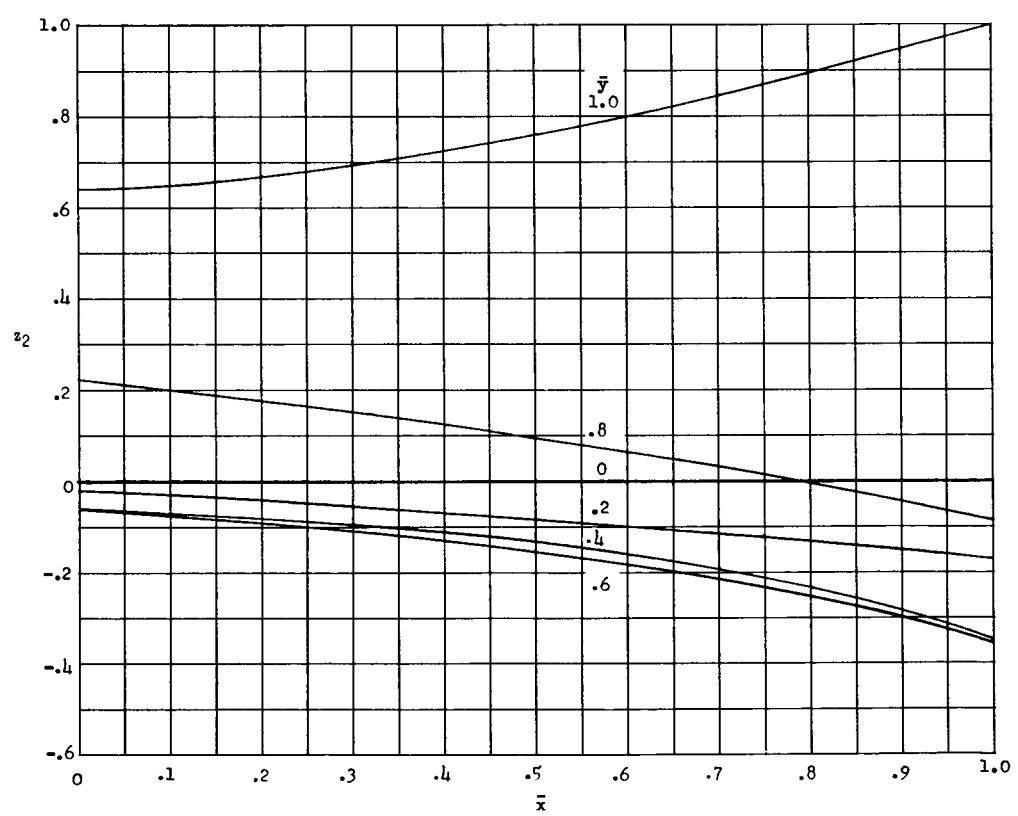
(b) Second mode.

Figure 5.- First three coupled vibration modes measured on model B.
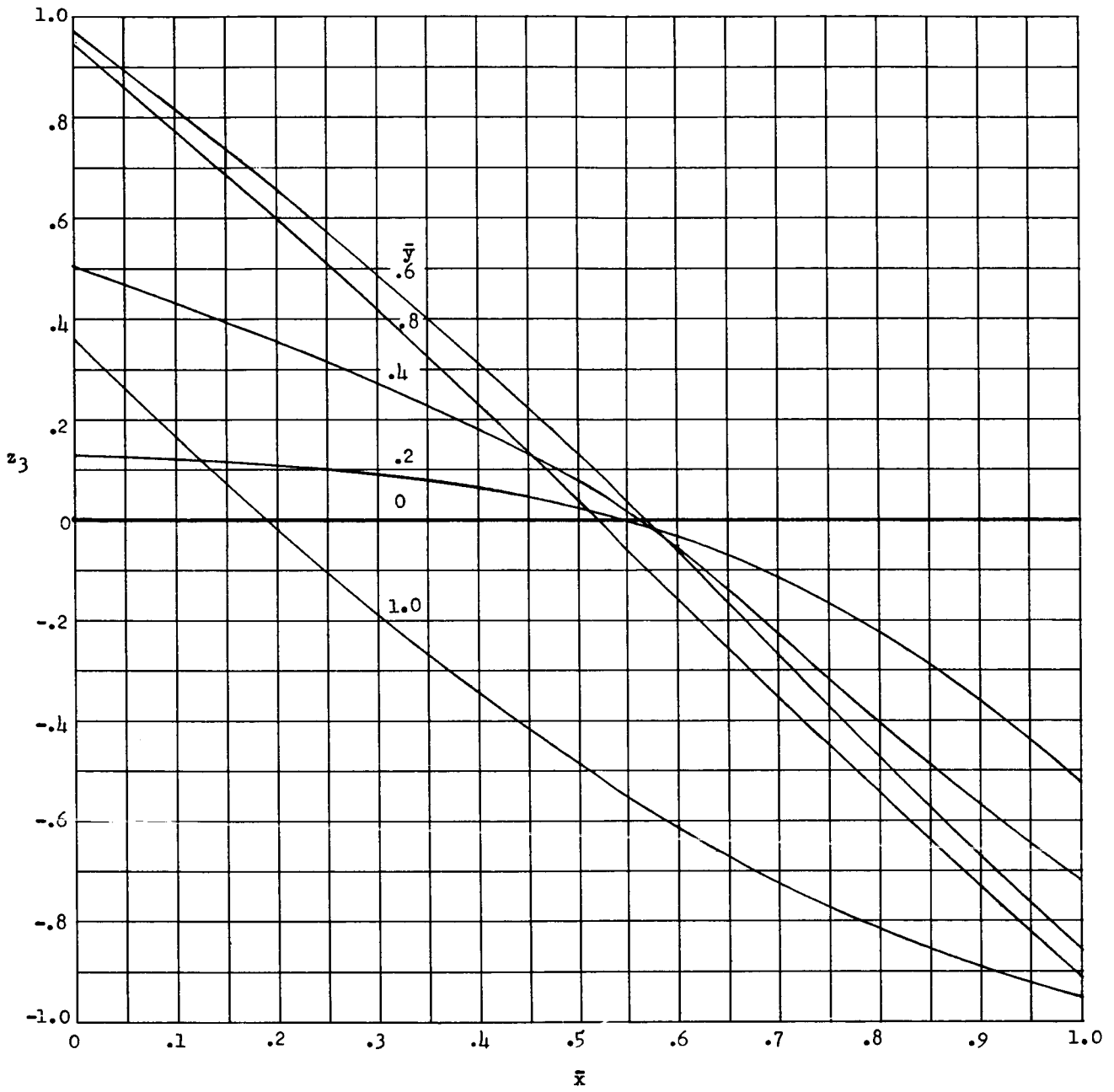
(c) Third mode.

Figure 5.- Concluded.
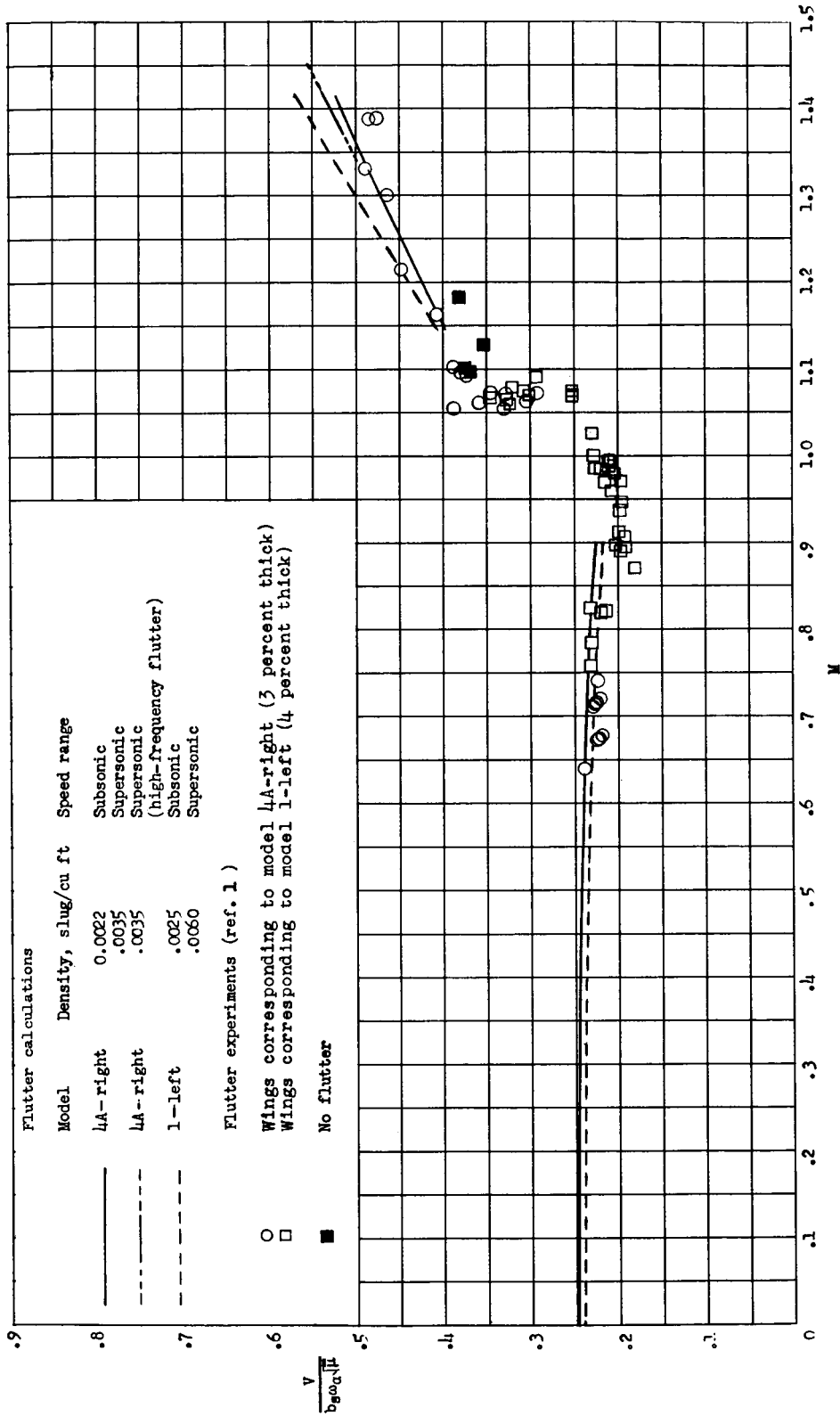
Figure 6.- Final results: Variation of flutter-speed coefficient with Mach number for model 1-left and model 4A-right. All calculations were made by modified strip method with three calculated uncoupled modes.

Flutter calculations

Model	Density, slug/cu ft	Speed range
4A-right	0.0022	Subsonic
	.0035	Supersonic
4A-right	.0035	Supersonic (high-frequency flutter)
1-left	.0025	Subsonic
	.0060	Supersonic

Flutter experiments (ref. 1)

O Wings corresponding to model 4A-right (3 percent thick)
□ Wings corresponding to model 1-left (4 percent thick)

$\frac{\omega}{\omega}$

M
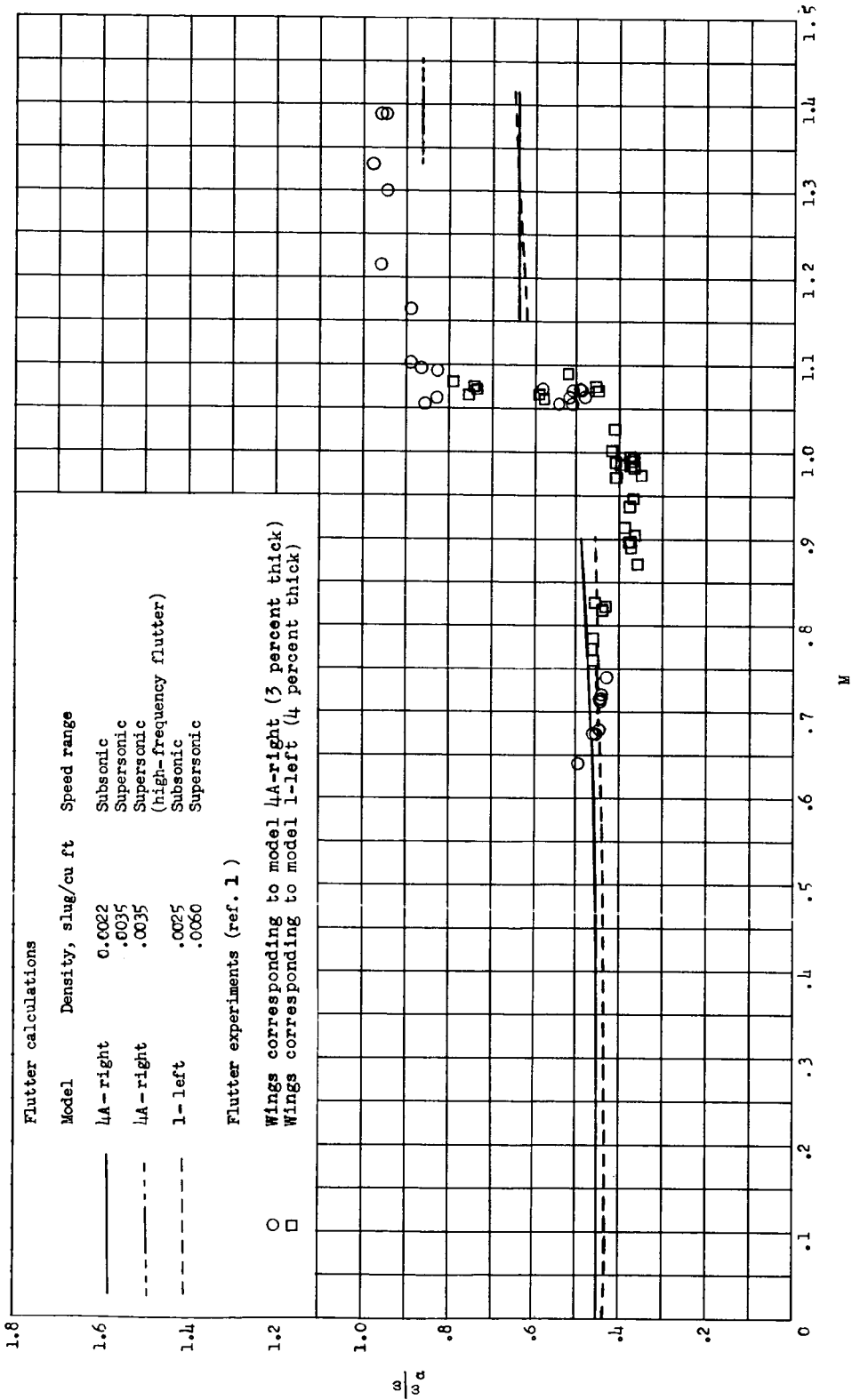
Figure 7.- Final results: Variation of flutter frequency with Mach number for model 1-left and model 4A-right. All calculations were made by modified strip method with three calculated uncoupled modes.
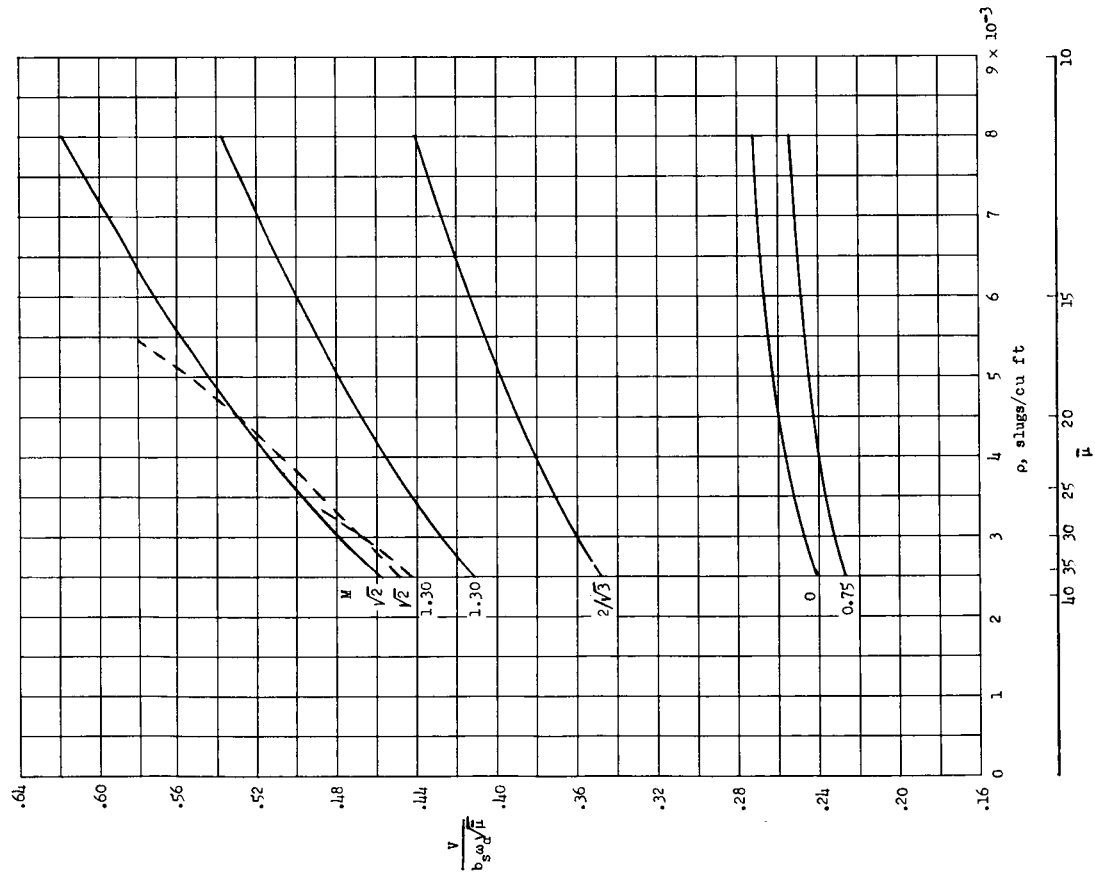
(a) Model 1-left.
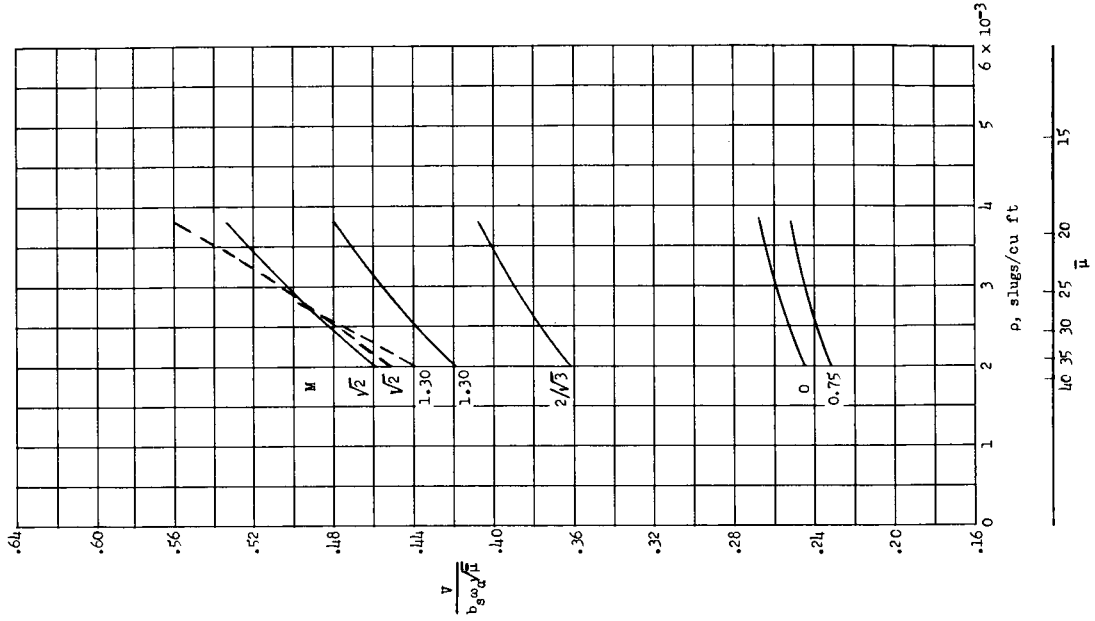
(b) Model 4A-right.

Figure 8.- Variation of flutter-speed coefficient with density for model 1-left and model 4A-right. Dashed curves represent high-frequency flutter boundary.
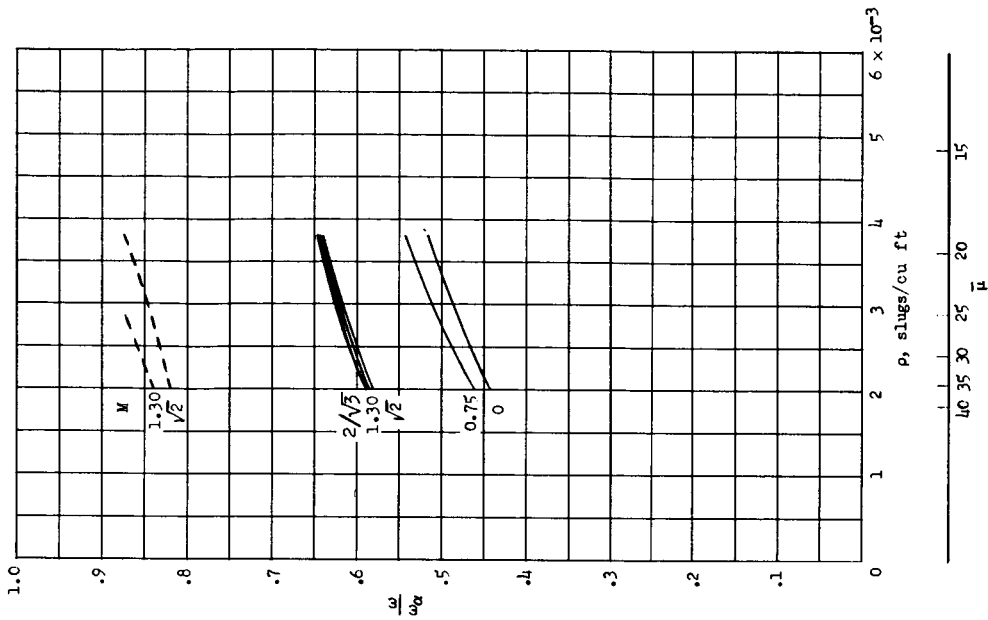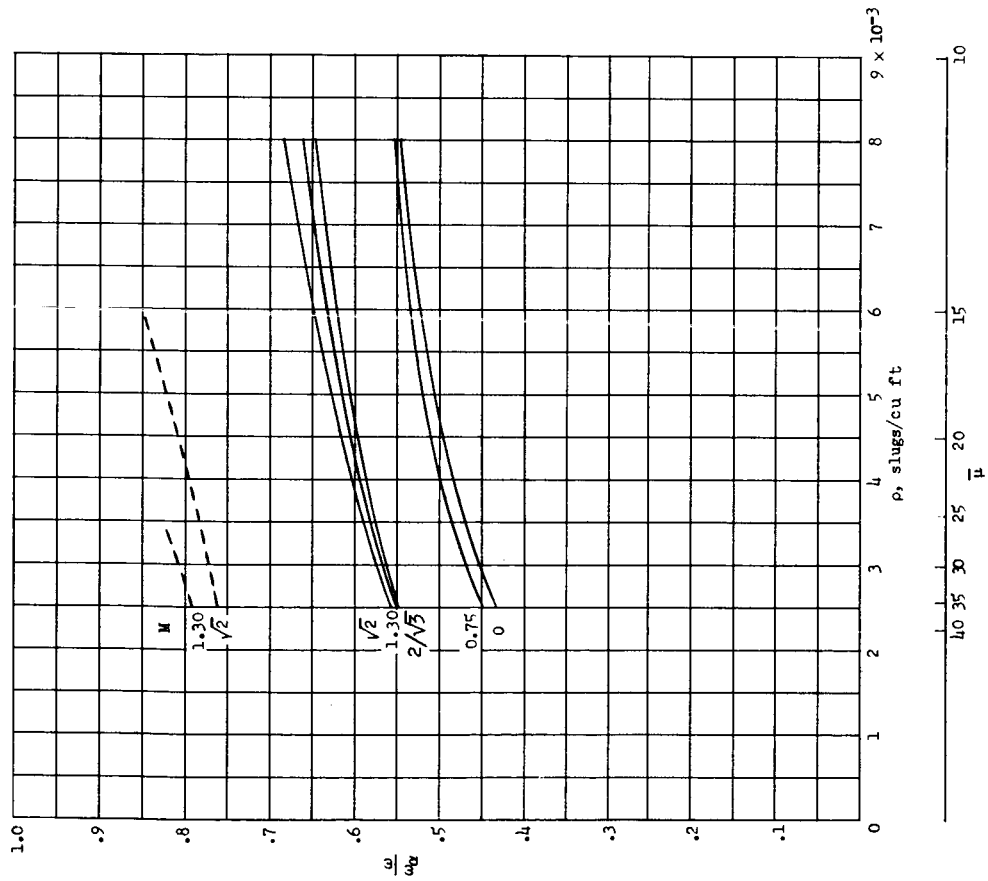
Figure 9.- Variation of flutter frequency with density for model 1-left and model 4A-right. Dashed curves are associated with high-frequency flutter boundary.
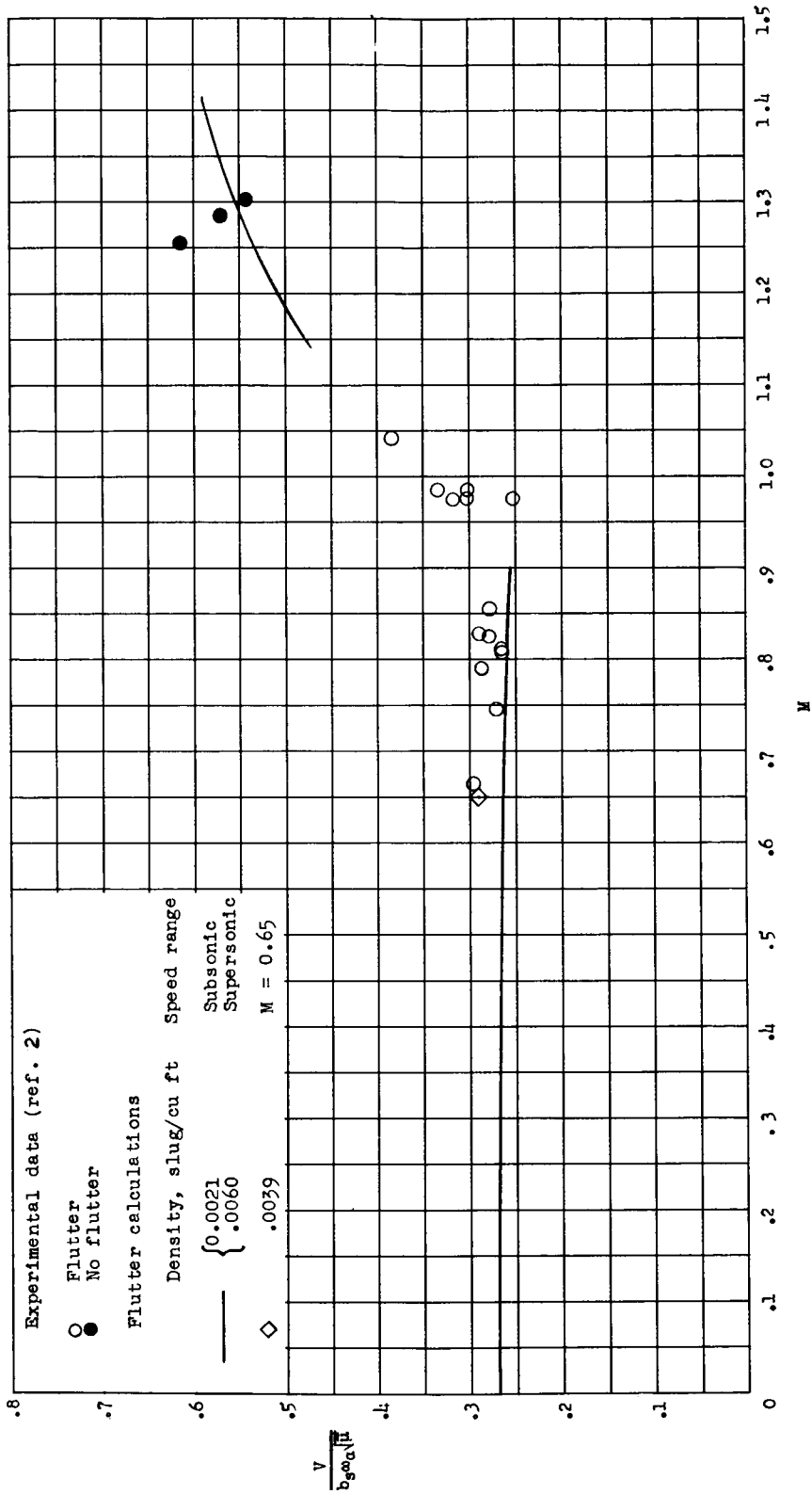
Figure 10.- Variation of flutter-speed coefficient with Mach number for model ballast I. All calculations were made by modified strip method with three calculated uncoupled modes.
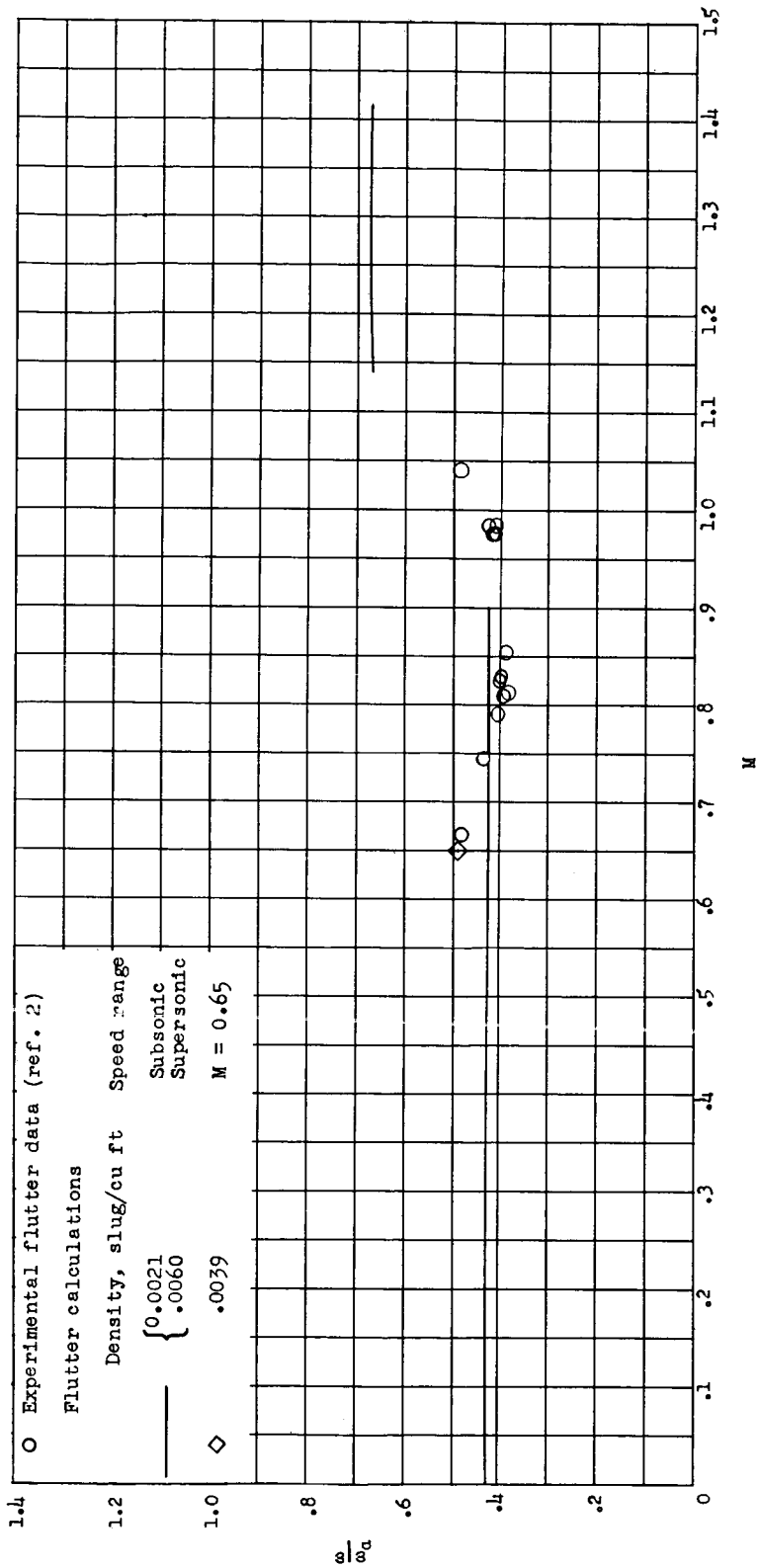
Figure 11.- Variation of flutter frequency with Mach number for model ballast I. All calculations were made by modified strip method with three calculated uncoupled modes.
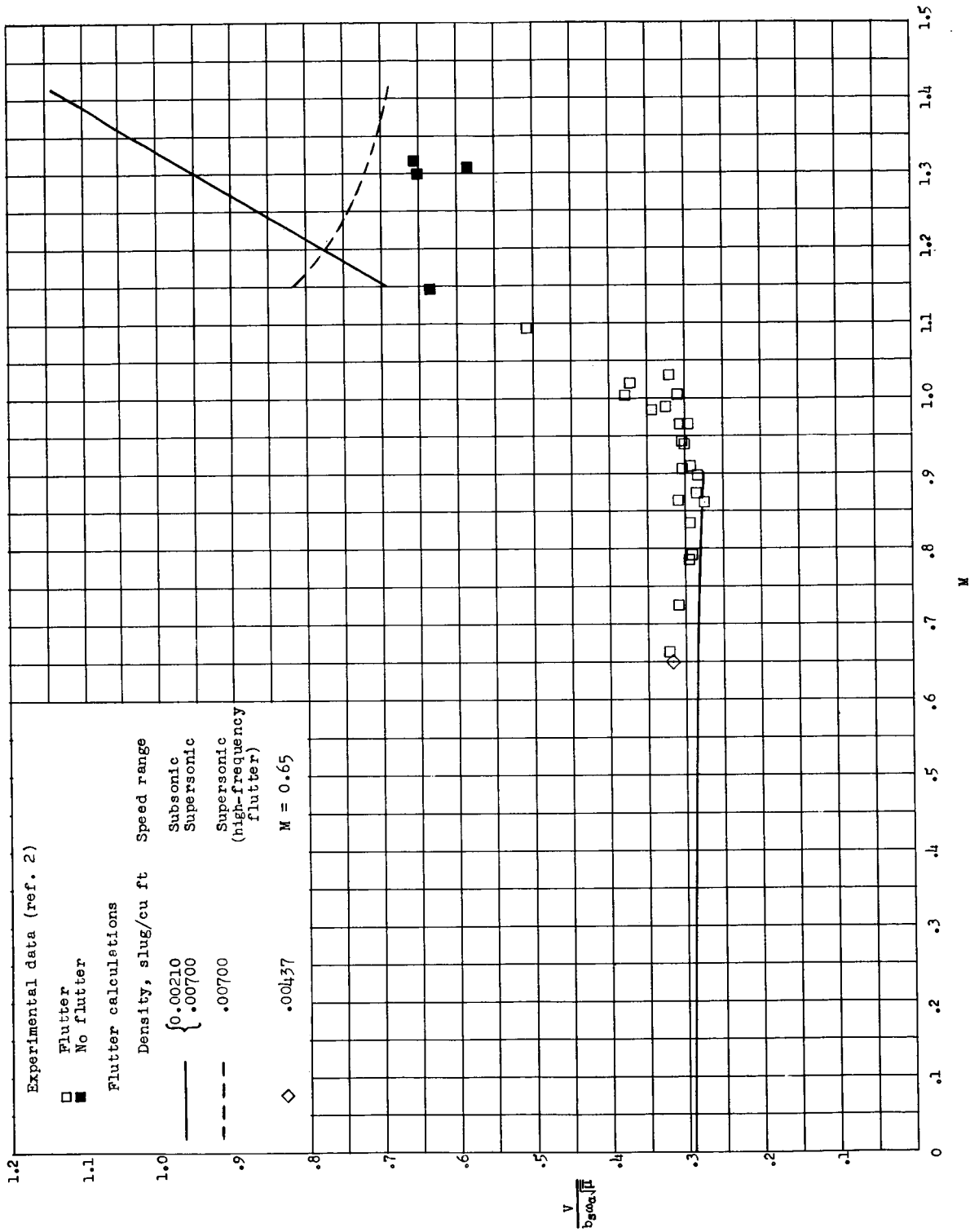
Figure 12.- Variation of flutter-speed coefficient with Mach number for model ballast II. All calculations were made by modified strip method with three calculated uncoupled modes.
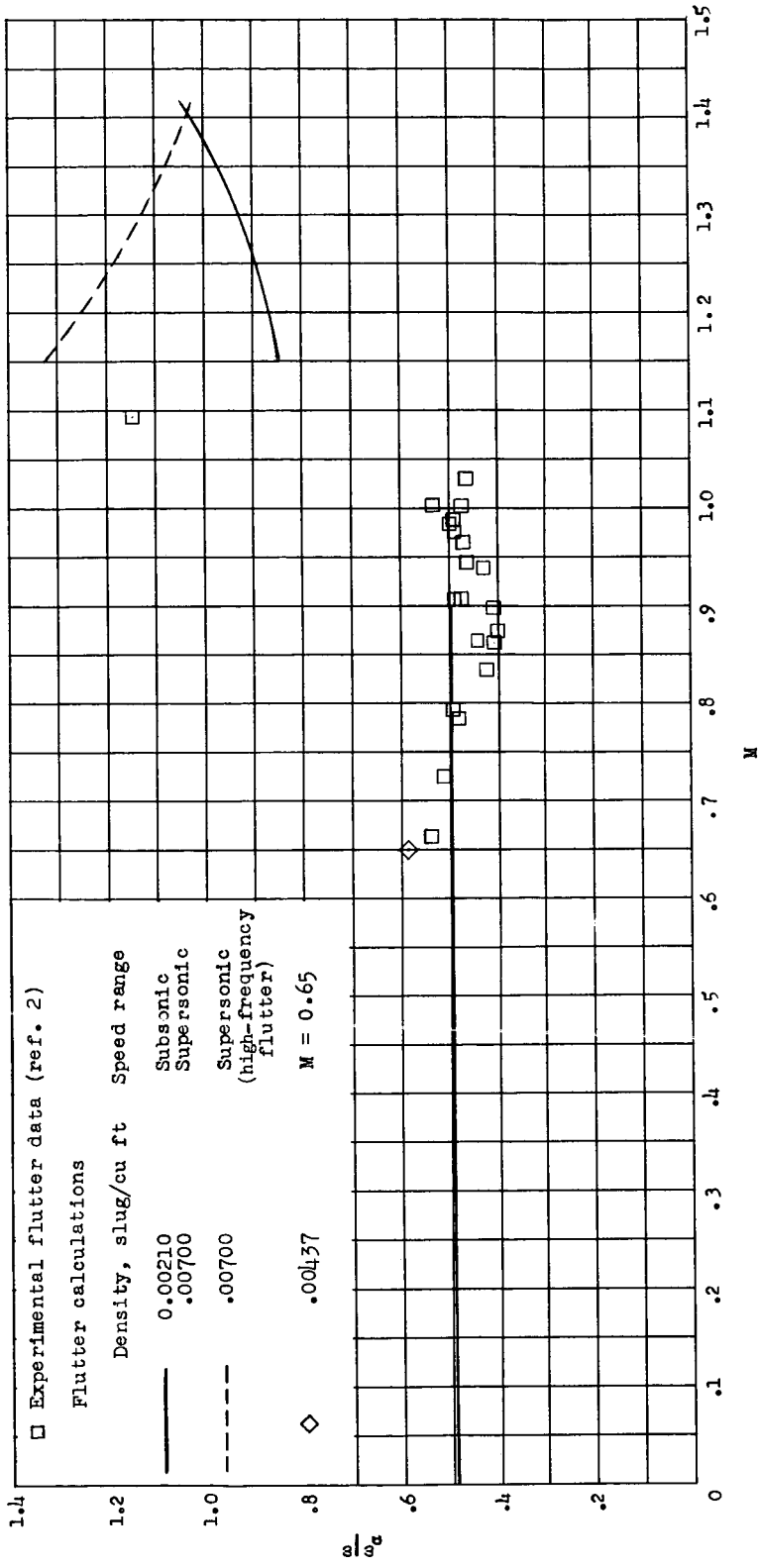
Figure 13.- Variation of flutter frequency with Mach number for model ballast II. All calculations were made by modified strip method with three calculated uncoupled modes.

51

Flutter calculations

Model	Density, slugs/cu ft	Speed range	Aerodynamic coefficients obtained from -
4A-right	0.0022	Subsonic	Linearized lifting-surface theory
4A-right	.0035	Supersonic	Linearized lifting-surface theory
4A-right	.0095	Supersonic (high-frequency flutter)	Linearized lifting-surface theory
B	Varies to coincide with experimental values	Supersonic	Linearized lifting-surface theory
B	.00089	M = 2.00	Second-order, lifting-surface theory

Flutter experiments

Wings corresponding to model 4A-right (5-percent-thick wings from ref. 1)
Wings corresponding to model 1-left (4-percent-thick wings from ref. 1)
Wings corresponding to model B (4-percent-thick wings from unpublished data)

No flutter

Sonic leading edge

$\dfrac{V}{b_s \omega_\alpha \sqrt{\mu}}$

M

Figure 14.- Comparison of flutter-speed coefficients calculated by modified strip analysis with experimental values for models tested in two wind tunnels. All calculations use three calculated uncoupled modes.
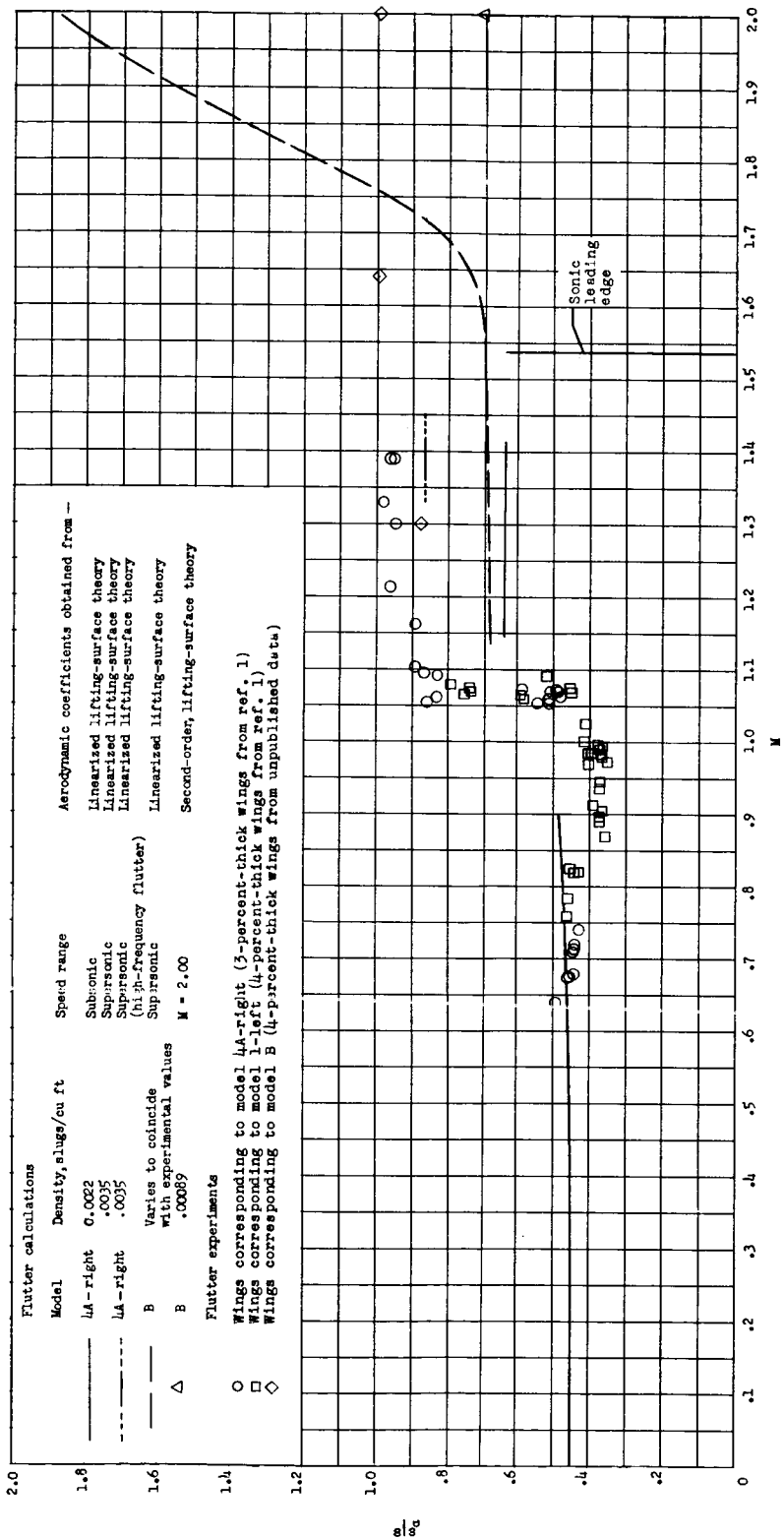
Figure 15.- Comparison of flutter frequencies calculated by modified strip analysis with experimental values for models tested in two wind tunnels. All calculations use three calculated uncoupled modes.
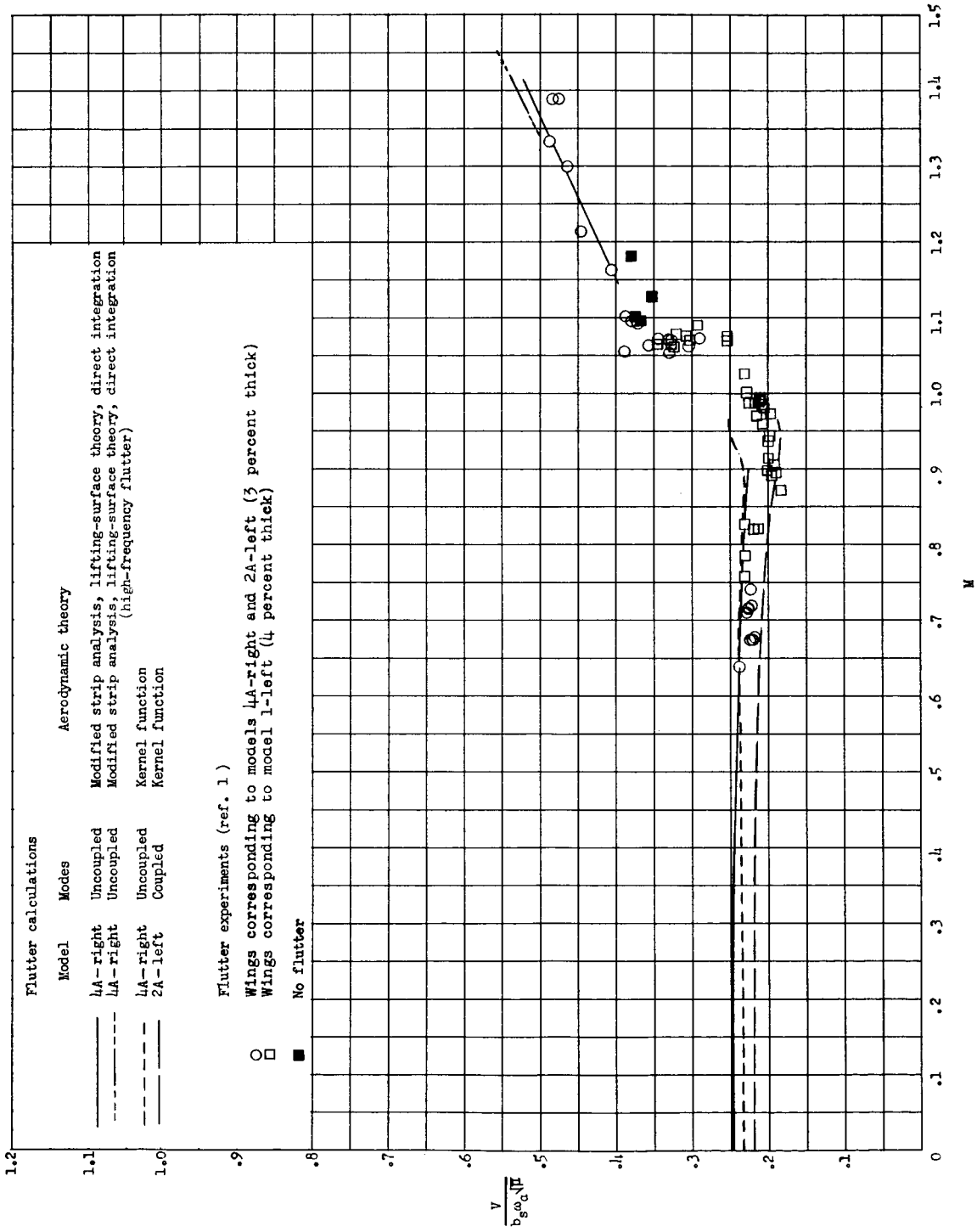
Figure 16.- Variation of flutter-speed coefficient with Mach number. Comparison of modified strip analysis with subsonic kernel function. All calculations use three calculated modes. For subsonic calculations, $\rho = 0.0022$ slug/cu ft; for supersonic calculations, $\rho = 0.0035$ slug/cu ft.
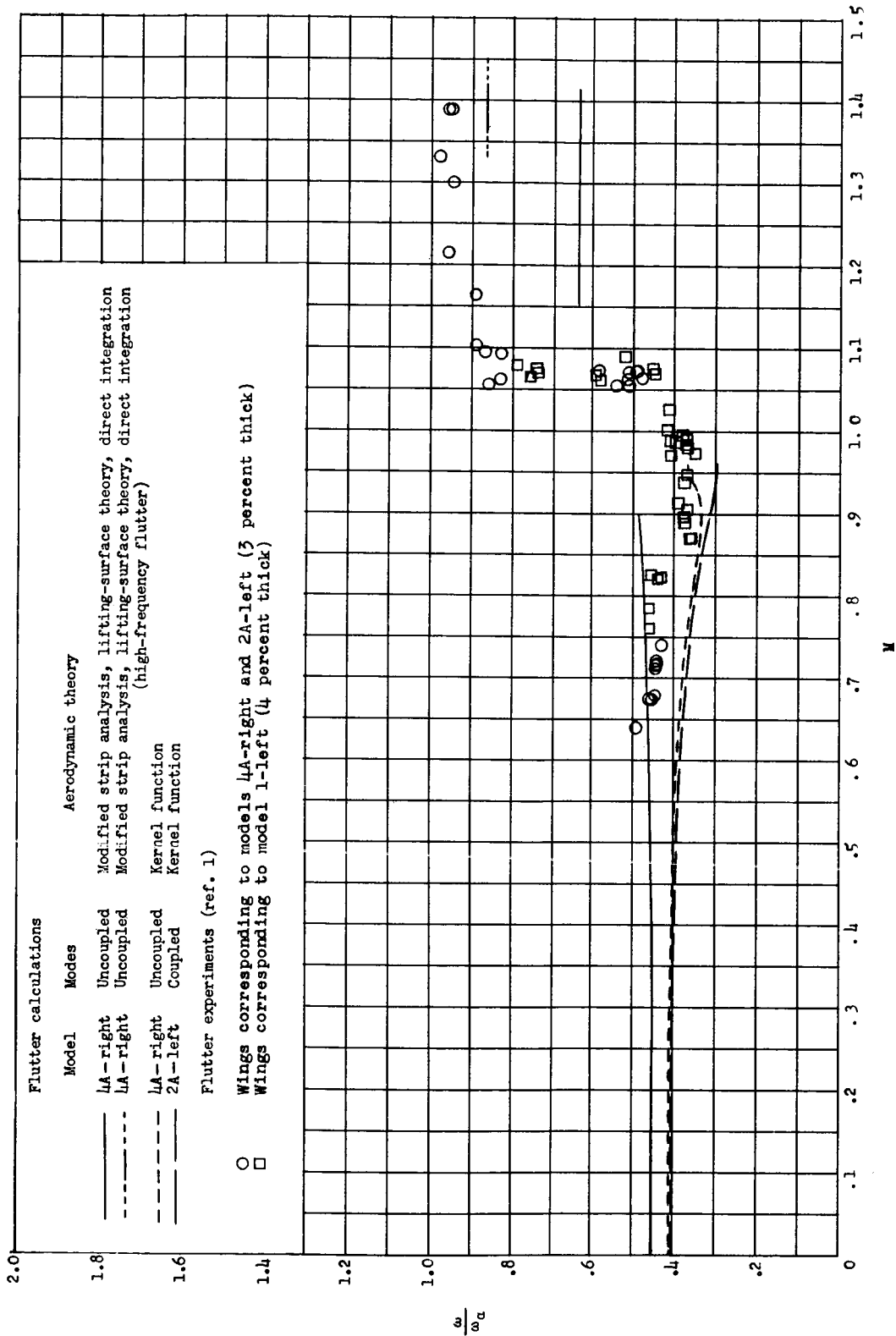
Figure 17.- Variation of flutter frequency with Mach number. Comparison of modified strip analysis with subsonic kernel function. All calculations use three calculated modes. For subsonic calculations, ρ = 0.0022 slug/cu ft; for supersonic calculations, ρ = 0.0035 slug/cu ft.
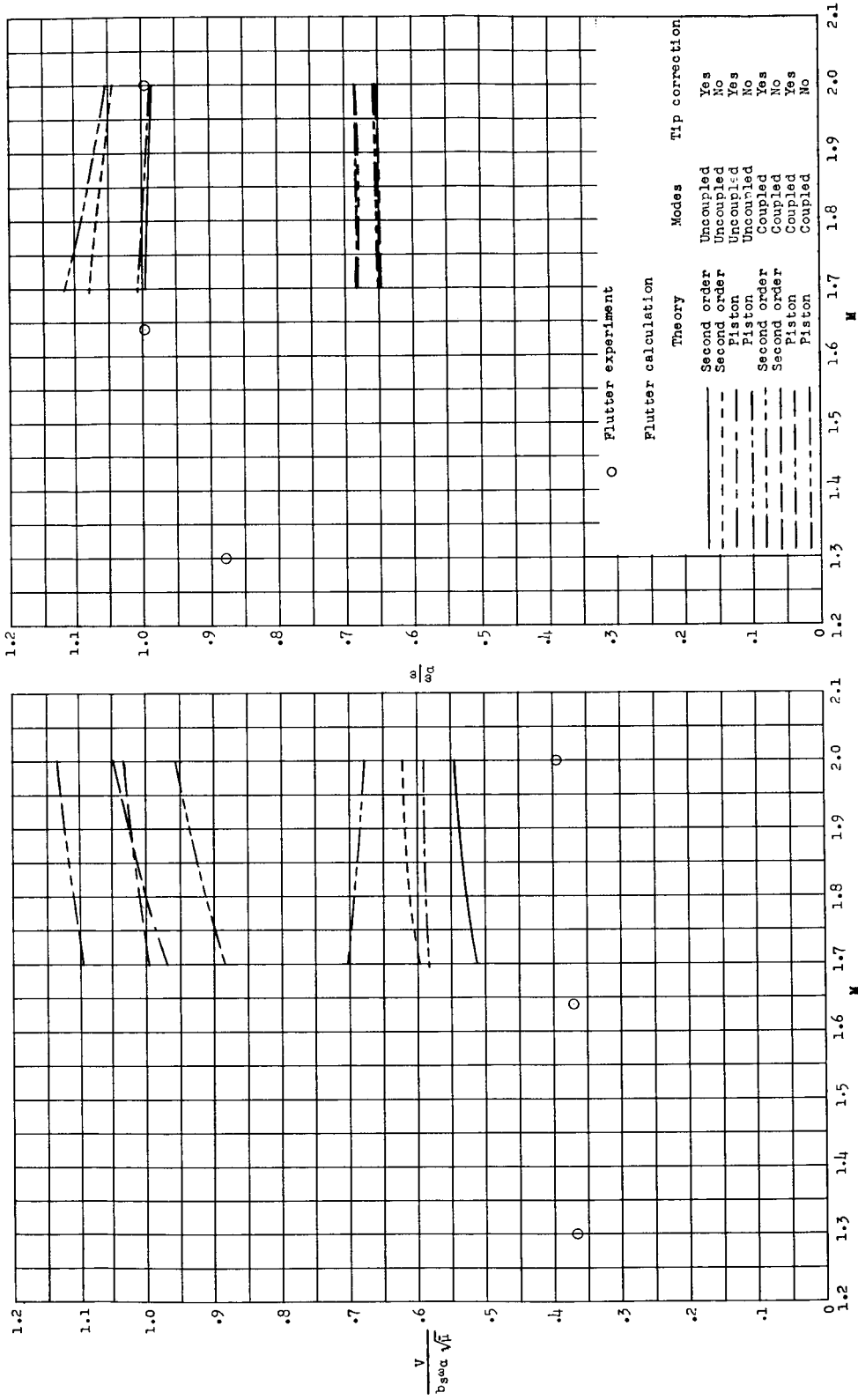
(a) Flutter-speed coefficients.

(b) Flutter-frequency ratios.

Figure 18.- Flutter characteristics for model B as obtained from piston theory and from quasi-steady second-order theory. All calculations use three calculated uncoupled modes or three measured coupled modes as indicated. Density varies linearly with Mach number from $\rho = 0.0009896$ slug/cu ft at $M = 1.7$ to $\rho = 0.0008900$ slug/cu ft at $M = 2.0$ in order to approximate experimental values.
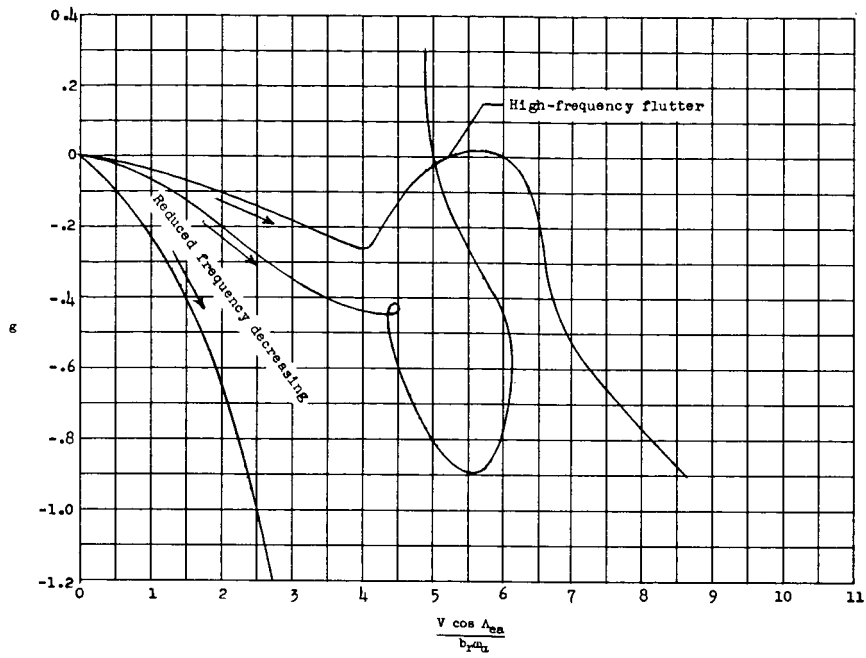
(a) $\rho = 0.0054$ slug/cu ft.
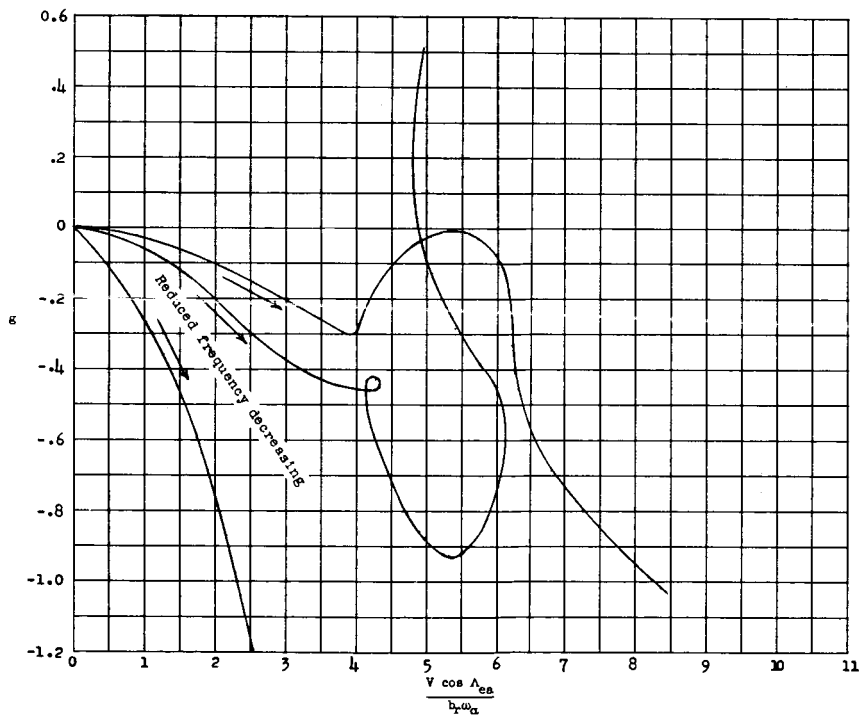
(b) $\rho = 0.0060$ slug/cu ft.

Figure 19.- Effect of flow density on high-frequency flutter boundary for model 1-left at $M = \sqrt{2}$.
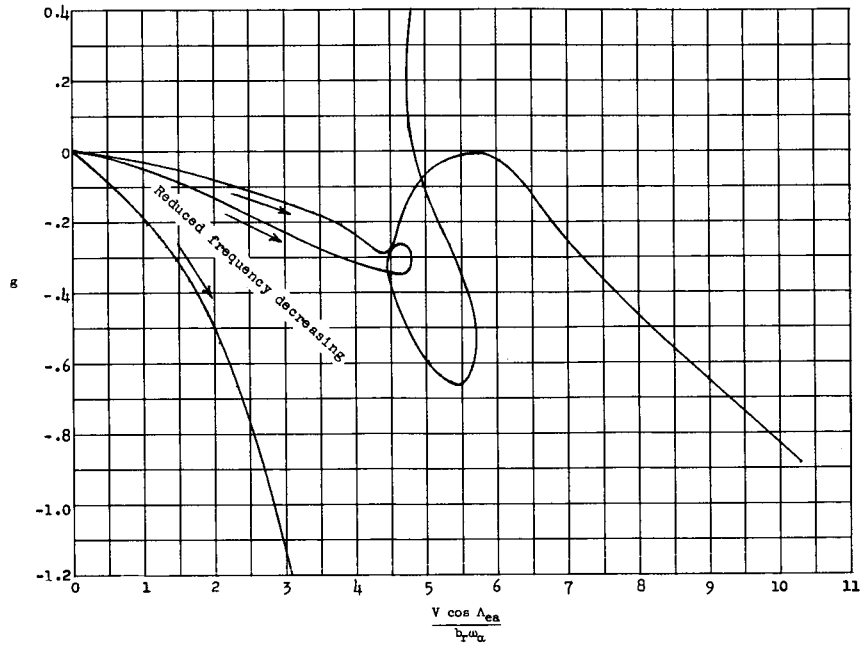
(a) M = 1.30.
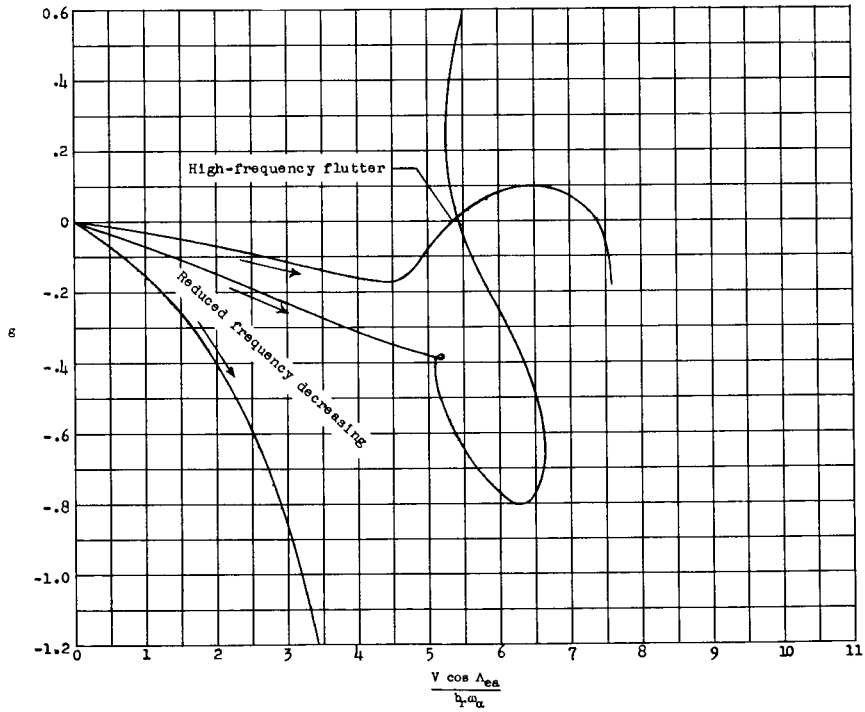
(b) M = $\sqrt{2}$.

Figure 20.- Effect of Mach number on high-frequency flutter boundary for model 1-left at ρ = 0.0038 slug/cu ft.
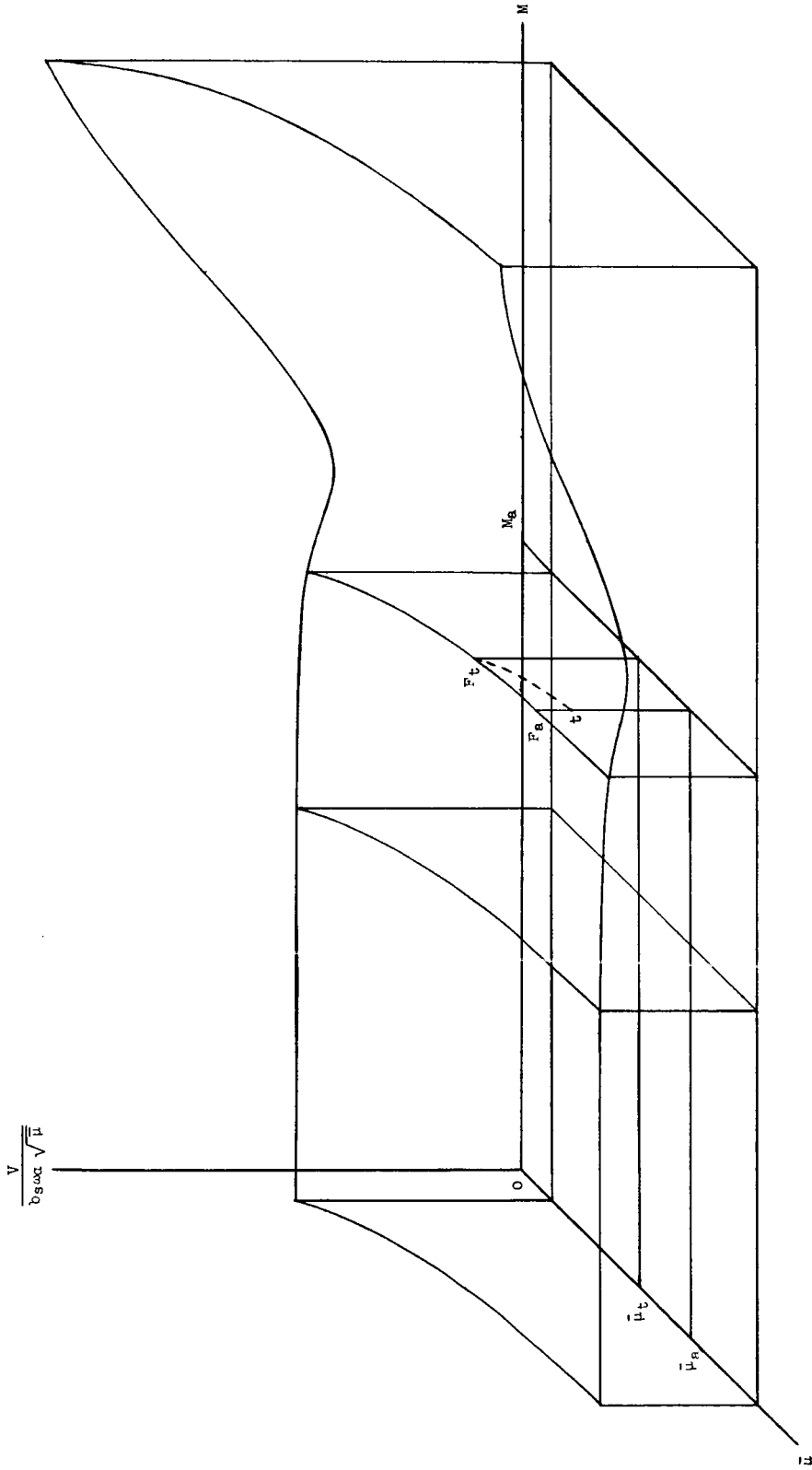
Figure 21.- Typical surface of flutter-speed coefficient as a function of Mach number and mass ratio.
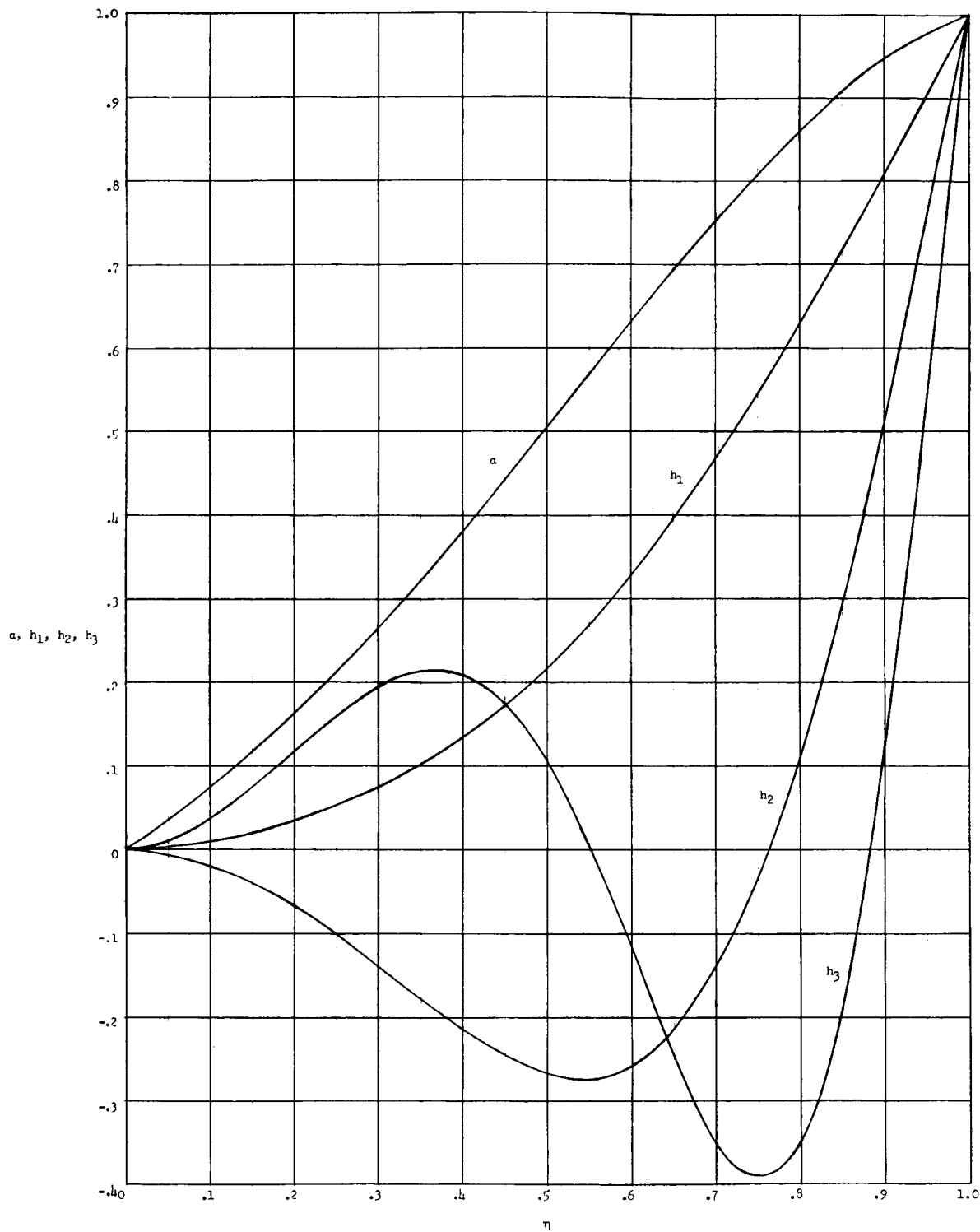
Figure 22.- Calculated uncoupled vibration modes for model 1-left.
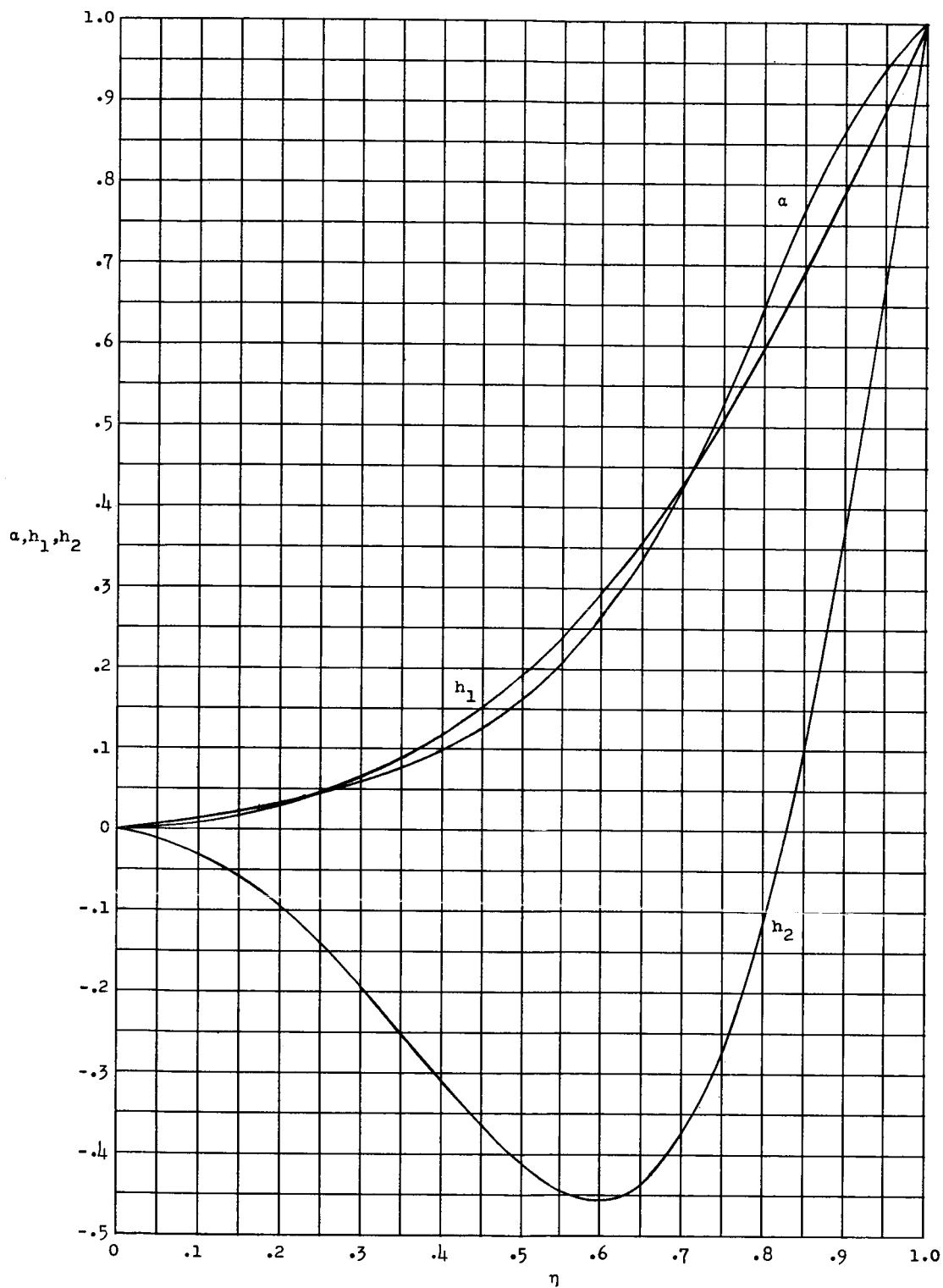
Figure 23.- Calculated uncoupled vibration modes for model ballast I.
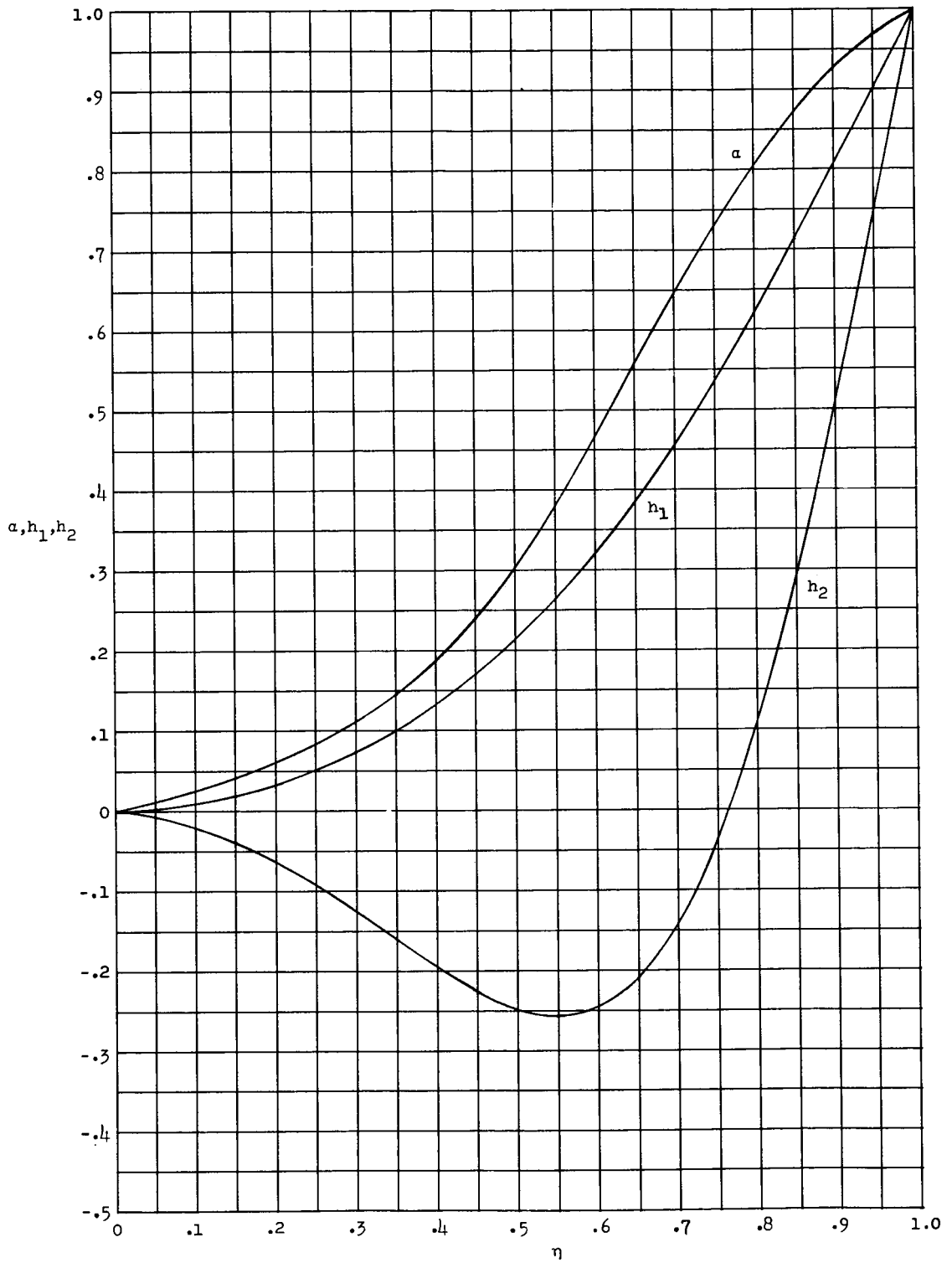
Figure 24.- Calculated uncoupled vibration modes for model ballast II.
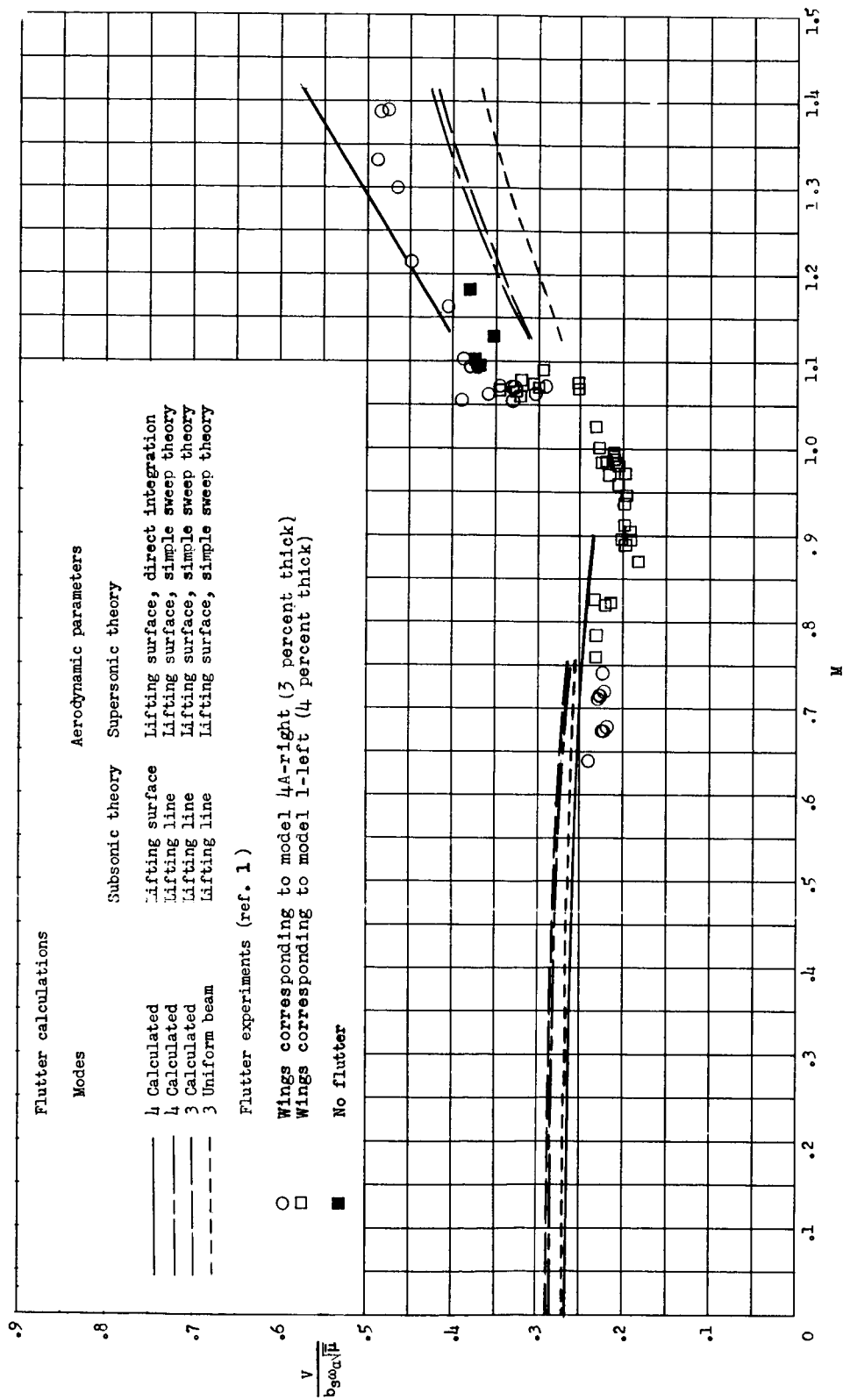
Figure 25.- Preliminary results: Variation of flutter-speed coefficient with Mach number. All calculations were made by modified strip method for model 1-left with $\rho = 0.0060$ slug/cu ft.
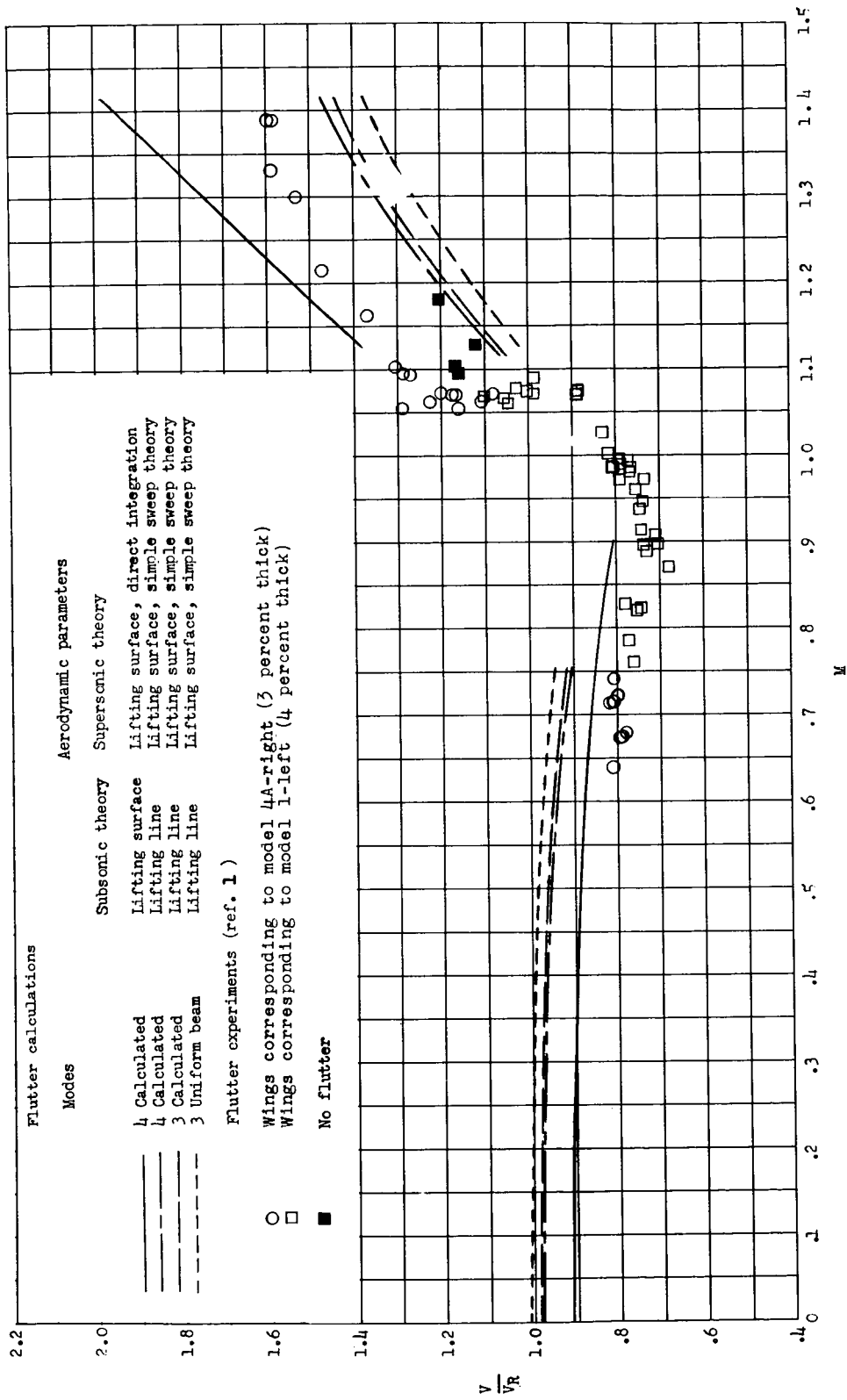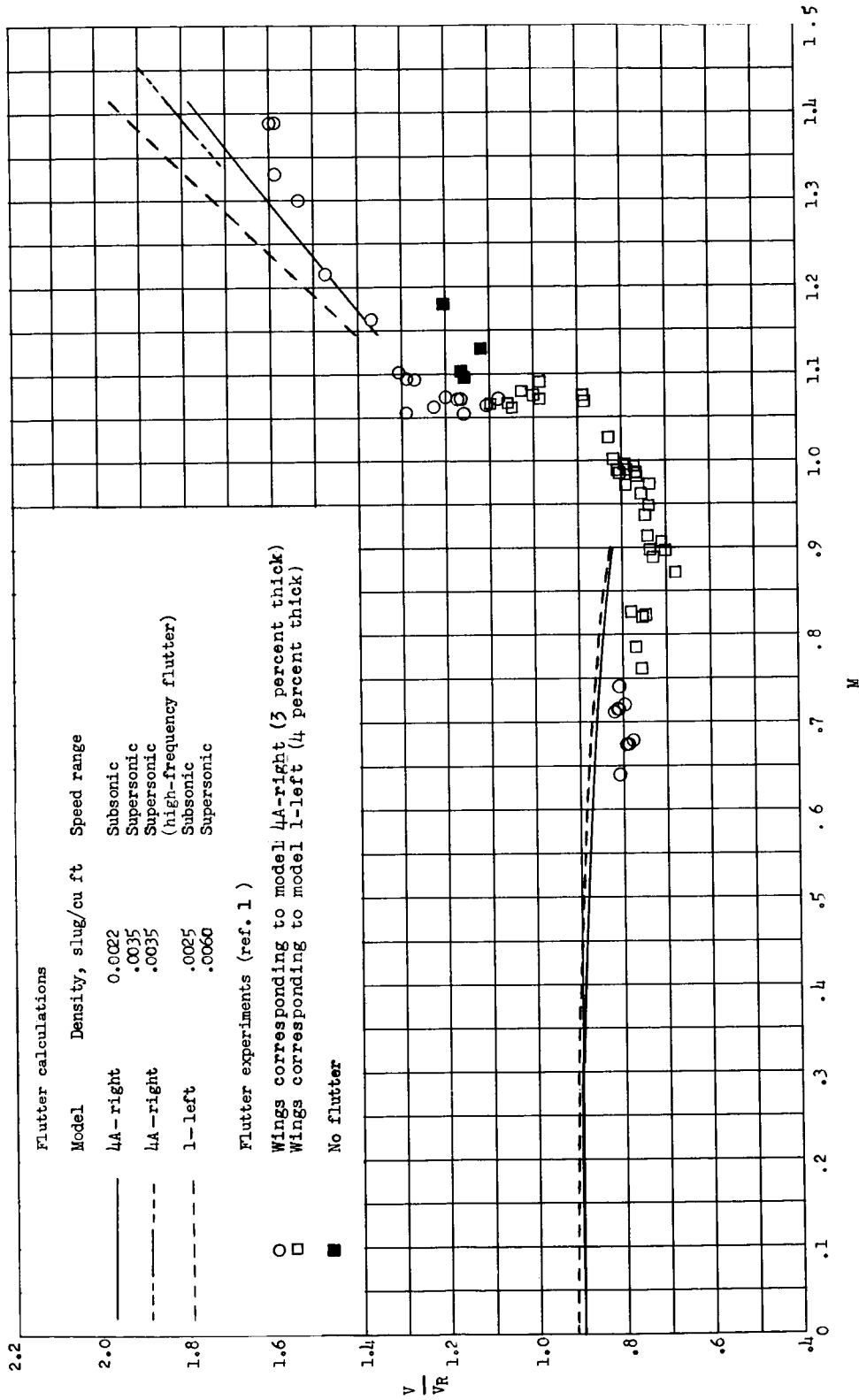
Figure 26.- Preliminary results: Variation of flutter-speed ratio with Mach number. All calculations were made by modified strip method for model 1-left with $\rho = 0.0060$ slug/cu ft.

64
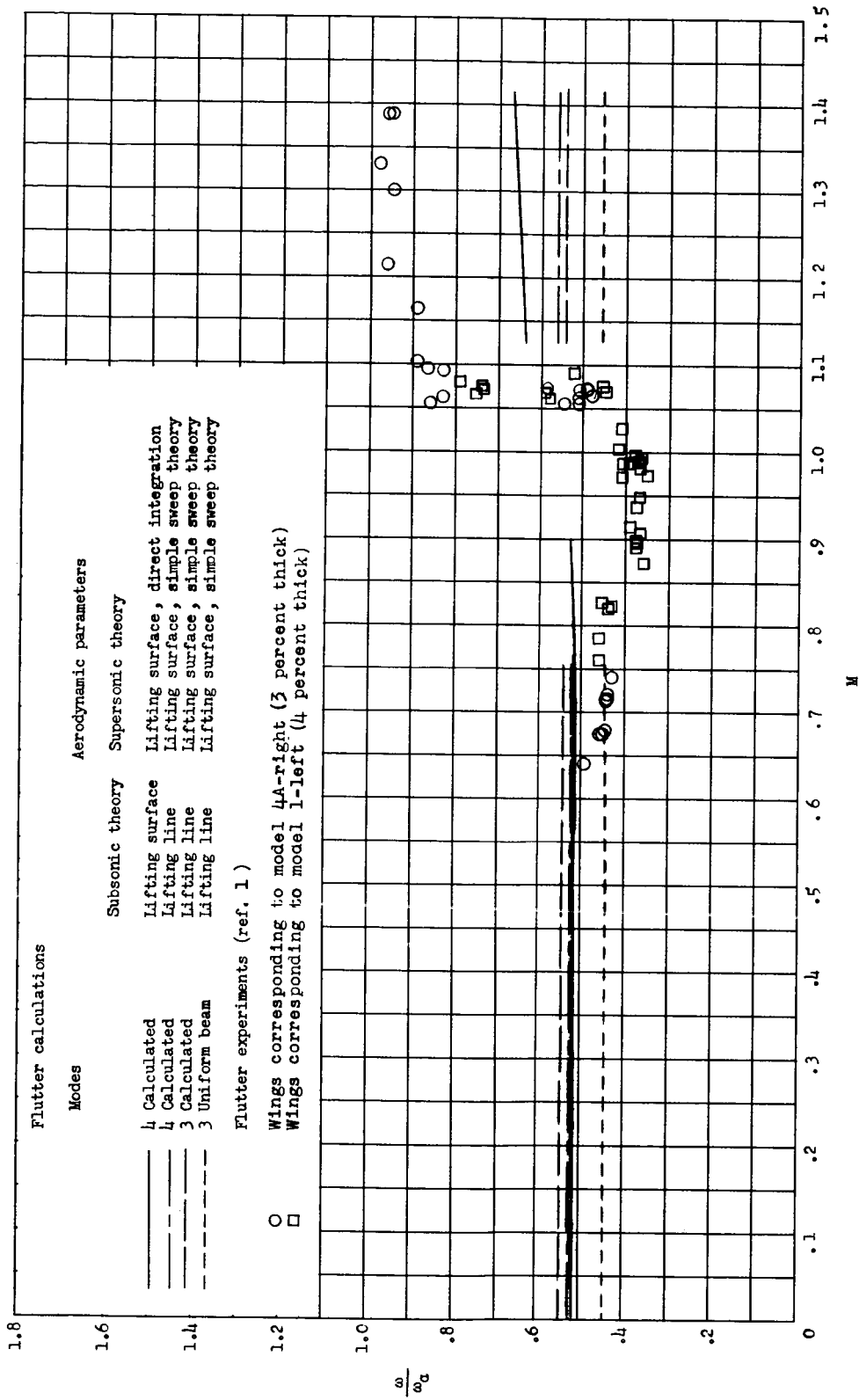
Figure 27.- Preliminary results: Variation of flutter frequency with Mach number. All calculations were made by modified strip method for model 1-left with $\rho = 0.0060$ slug/cu ft.
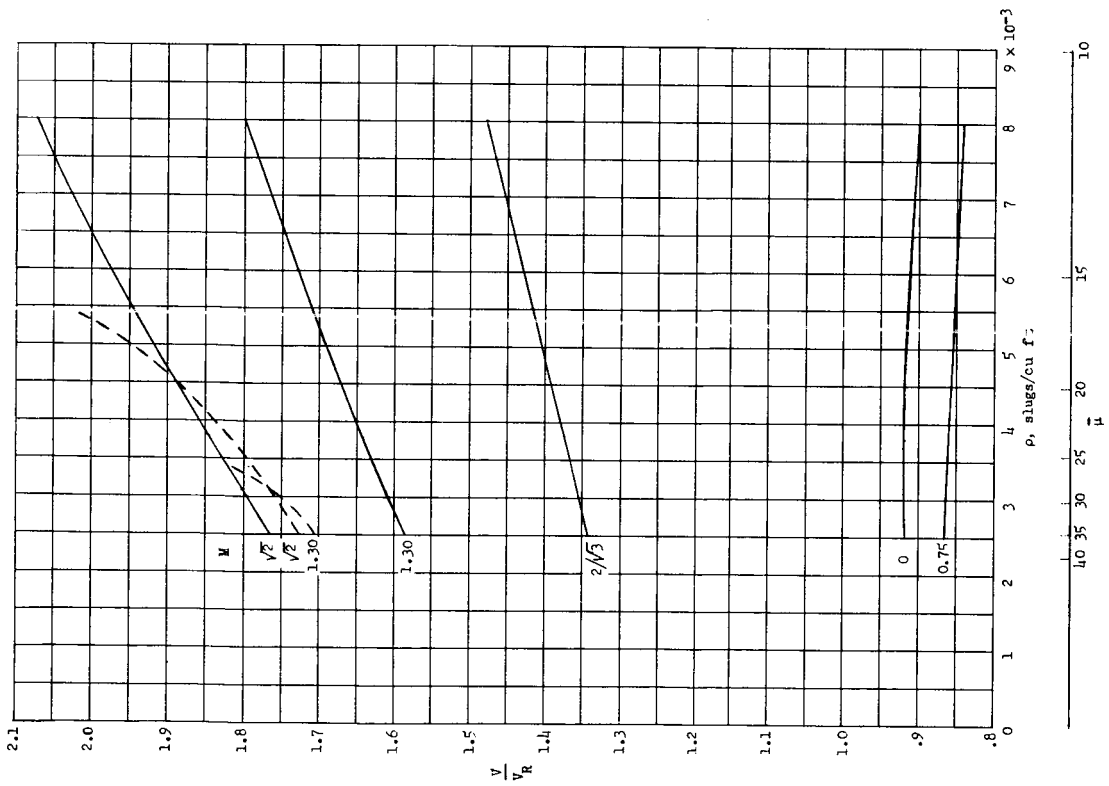
65

Figure 28.- Final results: Variation of flutter-speed ratio with Mach number for model 1-left and model 4A-right. All calculations were made by modified strip method with three calculated uncoupled modes.

66
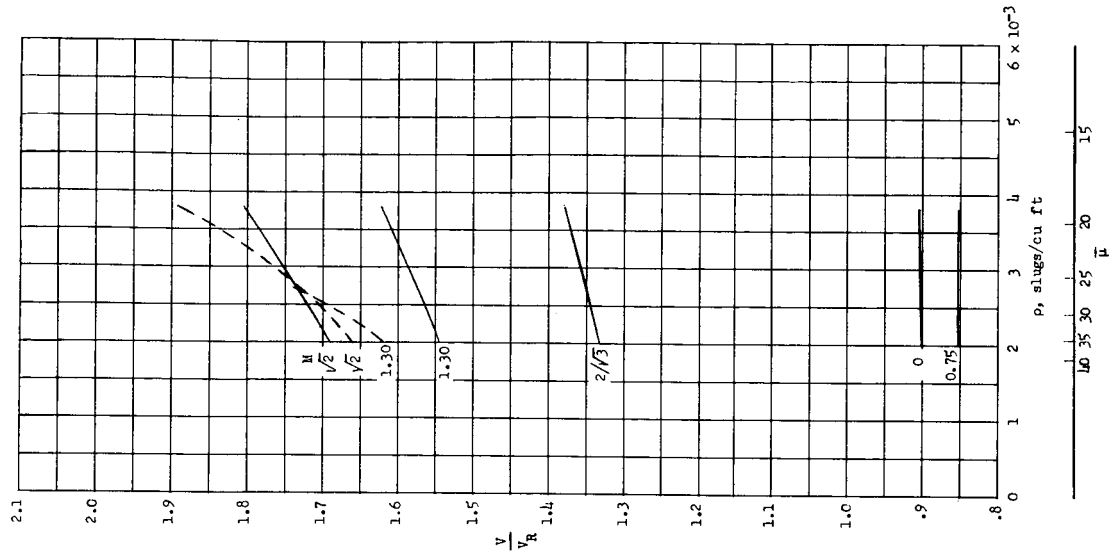
(a) Model 1-left.

(b) Model 4A-right.

Figure 29.- Variation of flutter-speed ratio with density for model 1-left and model 4A-right. Dashed curves represent high-frequency flutter boundary.
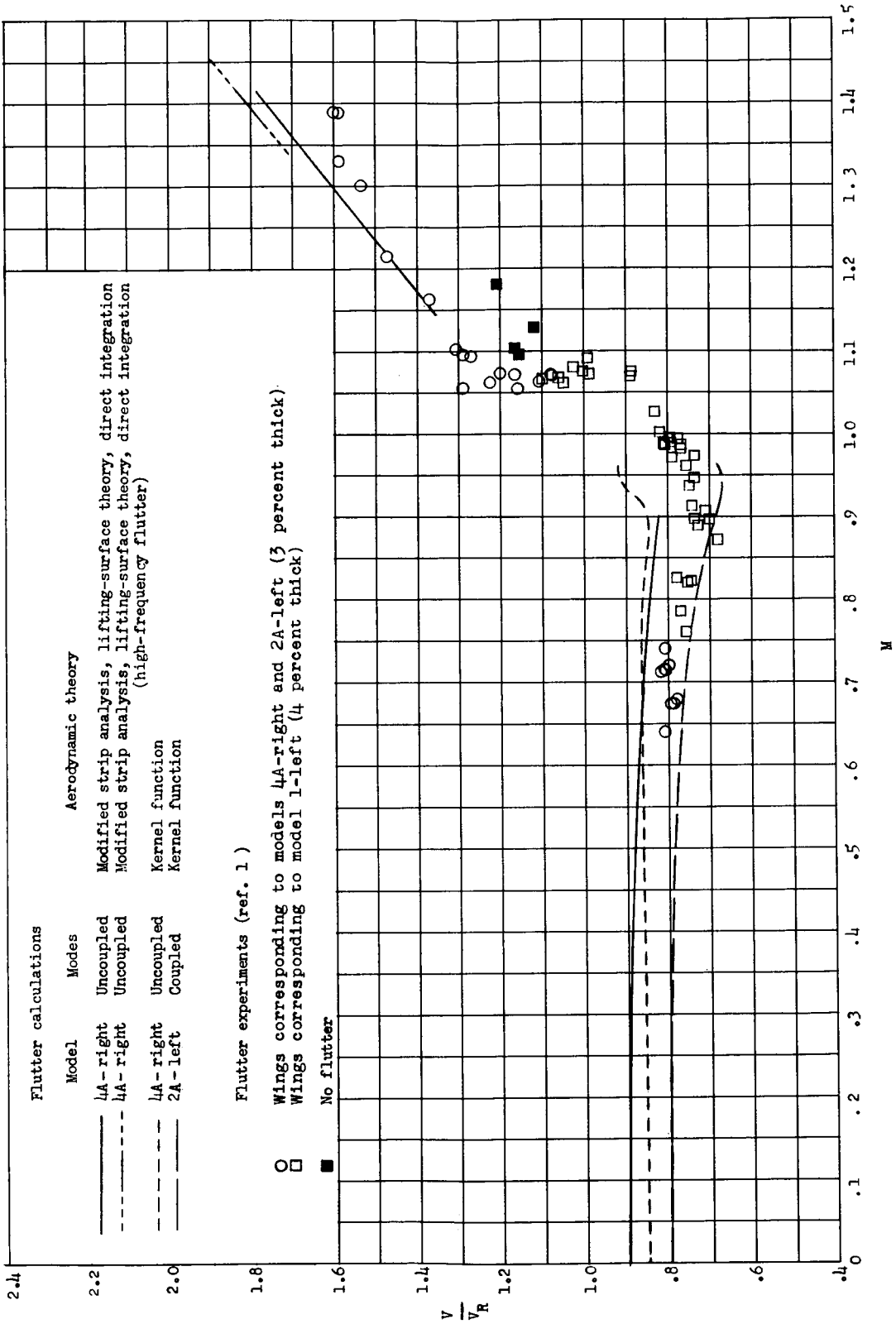
Figure 30.- Variation of flutter-speed ratio with Mach number. Comparison of modified strip analysis with subsonic kernel function. All calculations use three calculated modes. For subsonic calculations, ρ = 0.0022 slug/cu ft; for supersonic calculations, ρ = 0.0035 slug/cu ft.
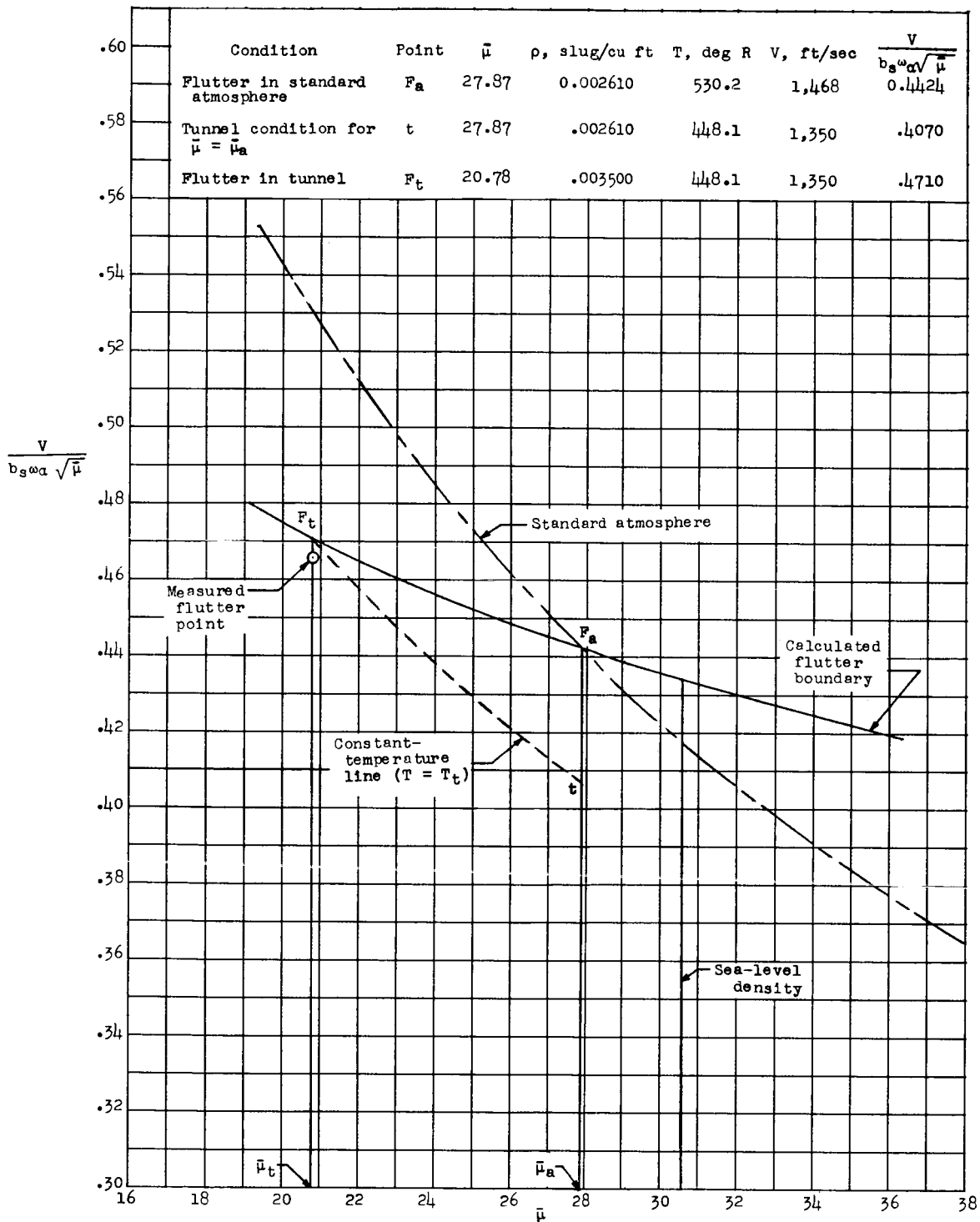
Figure 31.- Comparison of flutter boundary for model 4A-right at M = 1.30 with standard atmosphere and with conditions for Langley transonic blowdown tunnel.